Genome-scale Model Constrained by Proteomics Reveals Metabolic Rearrangements in the Heterologous Host *Streptomyces coelicolor*

Snorre Sulheim[1,2], Tjaša Kumelj[2], Dino van Dissel[1], Ali Salehzadeh-Yazdi[3], Chao Du[4], Kay Nieselt[5], Eivind Almaas[2,6], Alexander Wentzel[1], Eduard Kerkhoven[7,8,*]

1. Department of Biotechnology and Nanomedicine, SINTEF Industry, Trondheim, Norway
2. Network Systems Biology Group, Department of Biotechnology and Food Science, NTNU - Norwegian University of Science and Technology, Trondheim, Norway
3. Department of Systems Biology and Bioinformatics, Faculty of Computer Science and Electrical Engineering, University of Rostock, Rostock, Germany
4. Microbial Biotechnology & Health Programme, Institute of Biology, Leiden University, Leiden, The Netherlands
5. Integrative transcriptomics, Center for Bioinformatics, University of Tübingen, Tübingen, Germany
6. K.G. Jebsen Center for Genetic Epidemiology, Department of Public Health and General Practice, NTNU - Norwegian University of Science and Technology, Trondheim, Norway
7. Systems and Synthetic Biology, Department of Biology and Biological Engineering, Chalmers University of Technology, Göteborg, Sweden
8. Novo Nordisk Foundation Center for Biosustainability, Chalmers University of Technology, Gothenburg, Sweden

∗ Corresponding author

Abstract

Streptomyces coelicolor M1152 is a widely used host strain for the heterologous production of novel small molecule natural products, genetically engineered for this purpose through e.g. deletion of four of its native biosynthetic gene clusters (BGCs) for improved precursor supply. Regardless of its potential, a systems understanding of its tight regulatory network and the effects of the significant genomic changes in M1152 is missing. In this study, we compare M1152 to its ancestor M145, thereby connecting observed phenotypic differences to changes on transcription and translation. Measured protein levels are connected to predicted metabolic fluxes, facilitated by an enzyme-constrained genome-scale model (GEM), that by itself is a consensus result of a community effort. This approach connects observed differences in growth rate and glucose consumption to changes in central carbon metabolism, accompanied by differential expression of important regulons. Results suggest that precursors supply is not limiting secondary metabolism, informing that alternative strategies will be beneficial for further development of *S. coelicolor* for heterologous production of novel compounds.

Importance

This study provides the first systems description of *S. coelicolor* M1152, an engineered heterologous expression host widely used for the production and discovery of natural products. By combining time-

series proteomics and transcriptomics, batch fermentation data and genome-scale modelling we can connect observed phenotypes to known genetic modifications and find extensive metabolic rearrangements in the M1152 strain compared to the wild-type stain M145. We furthermore found that the rational strategy of enhancing precursor supply will surprisingly only have limited impact.

Instrumental to this study has been the genome-scale model that has allowed us to contextualize the transcriptional changes. To consolidate recent efforts in this field we reconstructed the consensus model Sco-GEM in an open-science framework. This approach facilitates further development by the research community in an organized manner, including version control, continuous integration and quality control and tracking of individual contributions.

Introduction

The bacterium *Streptomyces coelicolor* has been the *de facto* model actinomycete for the production and regulation of antibiotics (1). Being known for over 100 years, the interest in this organism predates the golden age of antibiotic research. With its complex life cycle, featuring mycelial growth and differentiation, spore formation, programmed cell death and the ability to produce multiple secondary metabolites; including calcium dependent antibiotic (CDA) and the conveniently coloured actinorhodin (Act, blue) and undecylprodigiosin (Red, red), it has assisted greatly in our understanding how streptomycetes sense their surrounding (2–6), activate their developmental cycle (7) and regulate the production of antibiotics (8, 9). Further aided by the publication of its genome sequence (10), the antibiotic coelimycin P1 (yellow), produced from the formerly cryptic polyketide gene cluster known as *cpk*, was added to this list (11), illustrating that even after the antibiotic golden age there still has been much to be discovered in this prolific genus. Today, the widespread use of *S. coelicolor* continues as a host for heterologous production of biosynthetic gene clusters (BGCs) (12–17). Heterologous expression is a powerful strategy for novel compound discovery from BGCs that are either natively silent or originate from an unculturable source (18). Both are large untapped resources of microbial biodiversity, nowadays made evident and accessible due to recent advances within the fields of metagenomics, molecular biology and bioinformatics (19).

The effectiveness of *S. coelicolor* as a heterologous production host rests on a metabolism that has evolved to provide the necessary precursors to produce a broad range of complex molecules. Many of these molecules are produced upon the organism experiencing nutrient-limiting conditions that lead to growth cessation and complex re-modelling of its metabolism (20). Metabolic switching in *S. coelicolor* M145 in response to phosphate and glutamate depletion has previously been studied in detail at a wide variety of metabolic levels (1–3), unravelling a complex sequence of switching events that ultimately lead to the biosynthesis of the antibiotics Act, Red and CDA. Coelimycin P1 production, however, appears to be independent of the major metabolic switch (8).

To improve *S. coelicolor* M145 as an expression host for heterologous BGCs, strain M1146 was created by subsequently removing its four major BGCs (*Act, Red, CDA* and *Cpk*) (Gomez-Escribano and Bibb, 2011). This should increase precursor availability for the production of a range of heterologous products and provides a cleaner background in analytics efforts to identify novel compounds. *S. coelicolor* M1152 is a derivative of M1146, featuring the C1298T point mutation in the *rpoB* gene, which encodes the beta subunit of RNA polymerase with documented positive pleiotropic effects on the production of heterologous compounds (13, 22). At the moment of writing, M1152 is a preferred general 'superhost' for heterologous BGC expression (12, 16, 23–25) and starting point for further strain development.

A hurdle in further development of *S. coelicolor* as a 'superhost' is the limited knowledge of M1152 metabolism and its regulatory system, even while insight can be gained from analysing snapshots of

gene expression levels during regular time intervals of a batch fermentation (26–30). Complementary to cataloguing gene expression is elucidation of the metabolic behaviour, which is inherently connected with enzymes catalysing most metabolic transformations. Leveraging this relationship, we can apply proteomics data as constraints (31) on a genome-scale metabolic model (GEM) of *S. coelicolor* to reveal how proteome rearrangements affect the metabolic fluxes during the different stages of growth and how the metabolism in *S. coelicolor* M1152 differs from its parent strain, M145.

GEMs are both valuable resources of strain-specific knowledge, mathematical models able to predict steady-state flux distributions, and frameworks for interpretation and integration of different 'omics' data, e.g. transcriptomics and proteomics (32). The increased interest in using genome-scale models of *S. coelicolor* is conspicious: since the first reconstruction in 2005 (33), five GEMs have been published (15, 34–37), and three of those within 2018: iKS1317 (15), Sco4 (37) and iAA1259 (35). Additionally, as a model organism for the *Actinomycetes,* the GEMs of *S. coelicolor* are frequently used as template for model development of closely related strains (38), such as *S. clavuligerus* (39), *Saccharopolyspora erythraea* (40) and *S. lividans* (41). The recent updates of the *S. coelicolor* GEM were developed in parallel by different research groups: while all groups share the common interest of utilizing a high-quality model for predictions and data analysis, the prevailing approach of independent parallel development is inefficient. Additional to duplicating a considerable amount of work, lack of common standards for documentation of progress and issues, evaluation of model performance, as well as the use of different annotations makes it cumbersome to compare and merge models.

To increase the rate and quality of model reconstruction, in this study two research groups of the Sco-GEM community, responsible for two of the latest model updates (15, 37), have joined forces to merge existing GEMs of *S. coelicolor* into one consensus-model that is publicly hosted on GitHub and can be continuously updated and improved by all members of the community. Hosting the model on GitHub has many advantages: 1) Open access and contribution; 2) Version control; 3) Continuous quality control with memote (42); 4) Continuous development and improvement; 5) New improvements released instantly (no publication lag time); 6) Complete documentation of model reconstruction. Such an approach has historic precedents: model reconstruction as a community effort has been a success for the human GEM (43), baker's yeast (44–49) and Chinese Hamster Ovary cells (50). The recent developments in *S. coelicolor* model and strain improvements in different research groups prove that it is an opportune time now to join forces in the *Streptomyces* modelling efforts as well.

Results

Reproducible reconstruction of Sco-GEM

We conducted a stepwise reconstruction of Sco-GEM, the consensus genome-scale metabolic model of *S. coelicolor*, while tracking development using Git for version control (**Figure 1A, Table S1**). Sco-GEM is the most comprehensive and highest quality GEM of this organism (**Figure 1B**), comprising 1777 genes, 2612 reactions, 2073 metabolites and a memote score of 77%, which is indicative of the overall model quality (42). Sco-GEM features accuracy of 96.5% and 74.5% (**Figure 1C**) in predicting correct phenotypes for growth environments and knockout mutants, respectively.

Sco-GEM has been reconstructed by curating the recently published iKS1317 model (15) to include genes, reactions and metabolites from the equally recently published models iAA1259 (35) and Sco4 (37). While the curations from iAA1259 were primarily related to coelimycin P1, butyrolactone, xylan and cellulose pathways, the 377 reactions added to Sco-GEM from Sco4 were scattered across a large range of different subsystems, covering both primary and secondary metabolism (**Figure S1**).

Subsequent to merging the existing *S. coelicolor* GEMs, we performed a number of further curations of the model: including improvement of annotations, both in terms of coverage and number of different databases, e.g. KEGG (51, 52), BioCyC (53), ChEBI (54) and MetaNetX (55). All reactions and metabolites have been given identifiers according to the BiGG namespace (56), and all reactions are categorized into 15 different subsystems, covering 128 different pathways.

The biomass composition was curated to reflect estimated levels of prosthetic groups that are associated to cellular proteins. Proteomics data, as discussed below, were used to estimate protein levels, while UniProt (57) provided annotations of proteins with prosthetic groups, which was used to estimate overall prosthetic group levels (**Table S2**).

Reaction reversibility updated for almost a third of queried reactions

The determination of reaction directionality and reversibility is an important step in a GEM reconstruction (58). However, the thermodynamic consistency of reactions was previously not considered in previous *S. coelicolor* models. We calculated Gibbs free energy changes for 770 of the 2612 model reactions (**Table S3**) using eQuilibrator (59), and inconsistencies in assigned reaction bounds transpired from a significant overlap of the range of Gibbs free energies between reversible and irreversible reactions (**Figure 1D**). A relatively lenient threshold of −30 kJ/mol was defined to classify a reaction as irreversible; with the intent not to over-constrain the model (**Figure 1E**). The proposed changes in reversibility were evaluated against growth and knockout data (15), discarding 59 of 770 the proposed reactions. Consequentially, the flux bounds of 273 reactions were modified, while all ATP-driven reactions were manually curated and generally assumed irreversible, unless they had an estimated positive change in Gibbs free energy or were known to be reversible. Examples of this include nucleoside diphosphate kinase (60) and ATP synthase (61).

Curation of transport reactions

As transport reactions have previously not been extensively curated in *S. coelicolor* models, we performed a thorough curation of transporters by querying various databases and BLAST analysis as detailed in Materials and Methods. This culminated in adding 43 new transport reactions and updating 39 of the 262 existing reactions in Sco-GEM (**Figure 1F, Table S4**). The majority of the transporters comprises primary active transport proteins and secondary carriers (46%), in accordance with previous work (62). Most primary active transporters are ATP-binding cassette (ABC) transporters (30%), while proton symports (30%) dominate the secondary carriers.

Development of the enzyme-constrained model EcSco-GEM

To include explicit constraints regarding enzymes catalysing metabolic reactions, the GECKO formalism (31) was applied to introduce enzyme turnover rates (k_{cat}) and prepare the model for integration of proteome data. The flux variability of the resulting enzyme-constrained model (EcSco-GEM) is strongly reduced compared to the classic genome-scale model (**Figure 1G**), as infeasible solutions due to limitation in protein allocation are discarded, significantly improving model predictions. From this, 17 time- and strain-specific EcSco-GEM models were generated by incorporation of estimated growth-, secretion- and uptake rates, as well as proteome data from cultivations that are detailed and analysed below.

Framework for further development of Sco-GEM by the community

The Sco-GEM model is hosted as an open repository as suggested by memote, a recently developed tool for transparent and collaborative model development (42). The memote tool is incorporated in the repository through Travis CI and tracks the model development on every change of the model. Sco-GEM v1.2.0 achieved a memote-score of 77%, which is superior to any previous model of *S. coelicolor* (**Figure 1B, Supplementary Information 1**).

Hosting Sco-GEM on GitHub with memote integration ensures continuous quality control and enables public insight into all aspects of model reconstruction and curation: any user can report errors or suggest changes through issues and pull requests. As contributions to the model development are fully trackable and can therefore be credited fairly, Sco-GEM is positioned as a community model that we envision to be continuously updated and widely used by the *S. coelicolor* research community.

In the remaining parts of the Results section, we have applied Sco-GEM along with transcriptome and proteome data, to study and compare the responses of *S. coelicolor* M145 and M1152 to phosphate depletion on a systems level and for the first time provide detailed insight into the distinct physiological features of engineered 'superhost' strain M1152, which will be of value for its further development.

The enzyme-constrained models connect regulatory changes in *S. coelicolor* M145 in response to phosphate depletion with metabolic fluxes

To evaluate whether the (Ec)Sco-GEM models can simulate behaviours of *S. coelicolor* metabolism, we performed and analysed time-course sampled cultivations of secondary metabolite producing strain M145 in the context of the generated models.

Batch fermentations of M145 undergoing phosphate depletion are highly reproducible.

S. coelicolor M145 was cultivated in batch fermentations using standardized protocols reported earlier (20). Cultures were sampled for 'omics data, as well as substrate utilization and secondary metabolite measurements to catalogue regulatory, proteomic and metabolic rearrangements during metabolic switching. The online and offline measurements showed that phosphate depletion in the cultivation medium was reached approximately 35 hours after inoculation, after which culture growth ceased and first compounds from the Red and subsequently the Act pathway were detected in the culture (**Figure 2A and 2B)**. Both D-glucose and L-glutamate were co-consumed, which continued after phosphate depletion, but remained in excess until the end of the cultivation after 79 hours. However, transition from exponential to stationary phase was accompanied by a 40% and 20% reduction in glucose and glutamate uptake rates, respectively. Note that *Streptomyces* can utilize intracellular phosphate storages after the medium is phosphate depleted (63). The transcriptome data was analysed in the light of previous studies (8, 9), and despite of the use of RNA-seq instead of microarrays and untargeted instead of targeted proteomics found to be in good agreement with the previous work (**Figure 2C and S2**).

Overall, the acquired cultivation and 'omics results are in very good agreement with previous results (8, 34), confirming the high reproducibility across independent cultivations and high reliability of the chosen cultivation and analysis procedures (**Figure 2**),rendering them a reliable baseline for comparison with respective data for M1152, as described below.

The EcSco-GEM models detail the production of the four major secondary metabolites by M145

The proteome data was incorporated into EcSco-GEM to yield time-specific metabolic models of M145, giving insight on how the metabolic activity in different pathways changed during the batch cultivation. Metabolic fluxes were estimated using an unbiased approach of random sampling, as alternative to assuming the optimization of a well-defined objective. A common assumption is that microorganisms have biomass yield as cellular objective, which can be used in linear optimization algorithms such as FBA (64). While it is feasible that *S. coelicolor* is wired to maximize its growth rate prior to phosphate depletion, but after the metabolic switch has taken place, it is difficult to define a clear objective. We applied an approach that samples the vertices of the solution space (65), and used their mean values to compare the metabolic fluxes both between the two strains and between different time points. The general overview from **Figure 2D** is an initial verification of the model: similar to how the metabolic

switch induces a large shift in global gene expression (8), the model predicts that the most drastic changes in fluxes in fact occur in response to phosphate depletion.

The response to phosphate depletion from the medium is coordinated by a set of PhoP regulated genes involved in phosphate metabolism (66–68), and the metabolic switch can be readily identified by the rapid upregulation of this regulon (**Figure 2C**), even while intracellular phosphate storages might be utilized. PhoP is also negatively regulating nitrogen assimilation, which can partly explain the reduced glutamate uptake after phosphate depletion (69), and upregulates biosynthesis of the secondary metabolites Act, Red and CDA (70–72). The bioreactor cultivations performed demonstrate this regulation in all layers of information: upregulation of the CDA and Red biosynthetic genes is observed at 37 hours after inoculation, while Act biosynthesis is initiated at 41 hours (**Figure 2F**). Measurable production in the culture commenced after 41 and 49 hours for Red and Act, respectively (**Figure 2B**). The enzyme-constrained models predict immediate increase in fluxes through the biosynthetic pathways for the four main compounds Act, Red, CDA and coelimycin P1 after the metabolic switch (**Figure 2D**). Note that the production of Red is fitted to measured, quantitative values, while this is not the case for Act, CDA and coelimycin P1.

The onset of secondary metabolism is strongly correlated with an increase in oxidative phosphorylation and a decrease in fatty acid biosynthesis.

The metabolic switch is concurrent with a decrease in fatty acid biosynthesis and an increase in oxidative phosphorylation and degradation of branched-chain amino acids, aminobenzoate and benzoate: the organism is attempting to reroute resources from primary to secondary metabolism (**Figure 2D and S3**). Although the revealed increase in oxidative phosphorylation is contrary to previous findings (73), an average 1.5-fold increase is observed in transcriptome analysis (**Figure S4A**) and the high correlation between oxidative phosphorylation and actinorhodin biosynthesis is supported by extra- and intracellular measurements (74): *S. coelicolor* is characterized by a high ATP/ADP ratio, demanding a highly active ATP synthase and electron transport chain. The model shows that the cofactors required to drive the electron transport chain and create the proton gradient are provided by an upregulation of citrate synthase, feeding acetyl-CoA into the TCA cycle (**Figure S4B**), as suggested earlier by Esnault et al. (2017) (74). The pentose phosphate pathway provides the main redox cofactor NADPH for polyketide biosynthesis, and its model-predicted flux increase upon initiation of polyketide synthesis is in agreement with previous studies (75, 76). The degradation of branched-chain amino acids (valine, leucine and isoleucine) provides precursors for secondary metabolism and the predicted increase concurrent with the onset of secondary metabolism is in line with previous observations (77). There is also a clear correlation between secondary metabolism and the metabolism of alanine, aspartate and glutamate, which are precursors for Red, CDA and Coelimycin P1 (**Figure 2D**), and similar observations are found in the antibiotic-producing *Amycolatopsis sp.* (78). Combined, the simulations of M145 show that the models are in good agreement with previously reported findings, validating that EcSco-GEM is able to capture *S. coelicolor* metabolic behaviour.

Model-assisted characterization of engineered *S. coelicolor* M1152 and its responses to phosphate depletion

As detailed above, EcSco-GEM shed new light on the metabolic switch in secondary metabolite producing strain M145. In contrast, *S. coelicolor* M1152 (13) is a M145 derivative void of the four major BGCs and featuring a point mutation in the *rpoB* gene. An enriched understanding of M1152 metabolism would benefit its further development. With this aim, we compared strains M145 and M1152 on the level of gene expression and metabolic fluxes.

M1152 shows reduced growth on phosphate limited medium

Batch cultivations of M1152 were performed using identical conditions and comparable sampling regimes as for M145 reported above. This enabled a direct comparison of the two strains at a systems level, revealing both expected and unexpected effects of the strains' genetic differences (**Figure 3**). As anticipated, the products of the Act, Red, CDA and Cpk pathways were undetectable in M1152 (**Figure 3A**). As previously observed (13), the growth rate of M1152 is reduced compared to M145 (0.15 h^{-1} vs 0.21 h^{-1} in the initial exponential growth phase), delaying phosphate depletion to 47 hours after inoculation (**Figure 3A**). The sampling time points for proteome and transcriptome were adjusted accordingly (**Figure 3B**), enabling pairwise comparison of measurements between the two strains. Genes responsive to phosphate depletion, part of the PhoP regulon (8), were used to align the different sample datasets for M145 or M1152 (**Figure 3C and S5**). PCA analysis of the proteome data confirms high consistency between corresponding biological replicates and incremental changes between sample points for both M145 and M1152 (mainly explained by PC1: 18.6% variance, **Figure 3D**). A clear strain dependent clustering of the data (PC2: 15.5% variance) indicates global differences at the protein level: EcSco-GEM was subsequently used to investigate the metabolic rearrangements in M1152 (**Figure 3E**).

M1152 and M145 differ significantly in central carbon metabolism

The glutamate and glucose consumption rates of M145 and M1152 imply substantial metabolic differences between the two strains prior to phosphate depletion. During cultivation on SSBM-P media, where glutamate is the sole nitrogen source, glucose and glutamate are co-consumed. M1152 has a reduced specific glucose uptake rate compared to M145 (**Figure S6A**), therewith obtaining a larger share of its carbon from glutamate (**Figure 4A**). Meanwhile, simulations with EcSco-GEM reveal that more than half of the glutamate-derived nitrogen is excreted as ammonia into the medium (**Figure S6B).** A reduced flux through glycolysis has previously been reported for strain M1146 lacking the four BGCs, and it is suggested that this is caused by allosteric inhibition of phosphofructokinase by a higher ATP/ADP ratio in the M1146 strain (74, 79). A possible explanation for the increased ATP/ADP ratio in strains lacking the Act cluster is that Actinorhodin downregulates oxidative phosphorylation (74).

The reduced uptake of glucose by M1152 propagates into central carbon metabolism (**Figure 4B**): a seemingly more active glycolysis in M145 leads to a predominant carbon flow towards acetyl-CoA and a higher excretion of acetate (**Figure S6B**). For M1152, however, EcSco-GEM reveals an increased flux from glutamate to alpha-ketoglutarate. Surprisingly, a major fraction of the alpha-ketoglutarate is subsequently converted by aspartate transaminase to oxaloacetate, resulting in the initial four steps of the TCA-cycle and the conversion of oxaloacetate to phosphoenolpyruvate by phosphoenolpyruvate carboxykinase carrying higher fluxes in M1152 than in M145 (**Figure 4B**). Another striking difference is that while ATP synthase activity is comparable between both strains, the M1152 model prefers NADH dehydrogenase channelling 3 protons (NADH17b) over the M145 model preferring cytochrome reductase and a NADH reductase channelling zero protons (NADH10b) for menaquinone reduction. The increased activity of NADH reductase in M1152 can be linked to oxidative stress (**Figure 4B**): the M1152 model predicts an increased flux through superoxide dismutase (SPODM) but not through catalase (CAT). This response is reflected in transcript levels (**Figure S7A and S7B**) and indicates that the reactive oxygen species produced by the NADH reductase is superoxide rather than hydrogen peroxide (80).

Redirection of malonyl-CoA as a result of Act, Red, CDA and Cpk BGC deletion

It is tempting to link the glycolytic redirection to the deletion of the main BGCs, as Act, Red and Cpk all use malonyl-CoA as a major precursor and redirection of malonyl-CoA from fatty acid synthesis towards secondary metabolism is a major event of the metabolic switch in M145. However, parts of

the response of M145 to phosphate depletion are retained in M1152 (**Figure 3E**): oxidative phosphorylation increases while fatty acid biosynthesis is downregulated, even though the process appears to be delayed in M1152. Considering the persistence of the metabolic switch in M1152, the fate of malonyl-CoA becomes unclear, as the downregulation of fatty acid biosynthesis remains even in the absence of alternative malonyl-CoA sinks of polyketide biosynthesis: little difference is observed between M145 and M1152 in both malonyl-CoA production and consumption (**Figure 5**). While fatty acid biosynthesis is strongly downregulated after the switch, this sink is still between 3 to 6 times larger than the total flux going into secondary metabolite biosynthesis. Consequentially, the predicted reduction in flux towards malonyl-CoA in M1152 is primarily affected by the reduced growth rate of this strain, while the absence of several biosynthetic pathways seems to have limited effect on the malonyl-CoA availability.

Transcriptome analysis reveal differential expression of global regulators

While the proteome data are an integral part of the EcSco-GEM models, RNA-seq data were used to both verify the trends and to gain further insights in the regulatory changes that are not captured by the metabolic models. Similar to the proteome, the RNAseq data showed large global differences between M1152 and M145, revealing 499 differentially expressed genes with a significance threshold of $p<0.01$.

Unsupervised clustering of the significantly changed genes reveal differences in regulatory systems related to redox regulation, signalling and secondary metabolism. The significantly changed genes were clustered into 7 groups with K-means clustering, with clusters 1-3 containing genes that are upregulated in M1152 compared to M145 and clusters 4-7 vice versa (**Figure 6A and Table S5**). A Gene Ontology (81, 82) enrichment analysis of each cluster shows that the majority of enriched processes are found in clusters upregulated in M145 (**Figure S8 and S9**, **cf. Figure 6A**). However, the few enriched processes upregulated in M1152 point to increased oxidative stress: antioxidant and peroxidase activity (SCO2634 [sodF]; SCO4834-35) in addition to biosynthesis of carotenoid (SCO0185–SCO0188), a known antioxidant (83, 84). The putative proteins within the cytochrome-P450 family (SCO7416–SCO7422) found in cluster 1 can be linked to increased oxidative stress (85), but also to oxidation of precursors used in synthesis of macrolides (86).

In cluster 2 we find *scbA* (SCO6266) and its downstream gene *scbC* (SCO6267), which stands out by being almost 6-fold upregulated in M1152. This high expression level is likely due to the deletion of *scbR2* (SCO6286), the last gene selected to be part of the *cpk* gene cluster (87). Besides regulation of the *cpk* cluster, ScbR2 binds upstream of several global regulators of development and secondary metabolism, including AfsK, SigR, NagE2, AtrA, and ArgR (88). It also acts together with ScbR to regulate ScbA, which produces the y-butyrolactone SCB1. Indeed, when looking at the genes associated with ScbR (88), AfsR (89) and AdpA (90), a clear difference in expression profiles of M145 and M1152 can be observed (**Figure 6B, S10A and S10B**), while this is not the case for genes associated with ArgR (**Fig S10C**).

Cluster 4 is enriched for genes that are related to the redox regulated transcription factor SoxR (91), and a similar pattern is observed for the entire SoxR regulon (**Figure 6C**). SoxR is known to react directly to the presence of actinorhodin (92, 93), and indeed, in M145 this group of genes follows the production profile of actinorhodin, while expression remains low in M1152. The SoxR regulon contains flavin and quinone reductases (91, 92), and it is suggested that these proteins reduce ATP generation by reducing the proton motive force (74). This is supported by the RNA-seq data where the ATP-synthase gene cluster (SCO5366–SCO5374) is upregulated almost 2-fold in M1152 compared to M145, most prominently in the stationary phase (**Figure S11A**). However, this upregulation is not evident from the proteome data (**Figure S11B**), explaining why the increased ATP synthase activity in M1152

is not captured by the EcSco-GEM predictions. Cluster 4 (**Figure 6C**) also contains the genes directly up- and downstream of the in M1152 deleted actinorhodin BGC (SCO5071–SCO5072 and SCO5091–SCO5092). In cluster 5, 6 and 7 we find genes with reduced expression in M1152, and the enriched processes are related to homeostasis, development, signalling and morphology. However, the connection to differences in observed phenotype or predicted metabolic states remains unclear.

Elevated expression of ribosomal proteins in M1152 after phosphate depletion

An increased transcription of genes encoding ribosomal proteins could be observed in M1152 after phosphate depletion (**Figure 6D**). While it may relate to the *rpoB* mutation, this observation contradicts the expected behaviour, which is a reduced expression of ribosomal proteins (94, 95): it has been suggested that the *rpoB* mutation mimics binding of ppGpp to the ribosomal subunit (22), while ppGpp is synthesized in response to nutritional stress and reduces transcription of genes related to growth, such as genes encoding rRNAs, in addition to development/differentiation and antibiotic production (96, 97). Nonetheless, the expression of the ppGpp regulon was not found to be significantly changed in M1152 (**Figure S12**).

Meanwhile, nucleoside triphosphate levels strongly regulate ribosomal RNA synthesis, and we therefore hypothesize that a higher ATP/ADP ratio in M1152 compared to M145 after phosphate depletion may be causing the differences in expression of ribosomal proteins. The observed upregulation of the ATP-synthase gene cluster supports this hypothesis (**Figure S11A**), and a high level of ATP has been reported in the M1146 strain parental to M1152 (98) which also lacks the 4 major BGCs but does not feature the *rpoB* mutation. Regardless, neither of these hypotheses can explain why a difference in ribosomal protein expression is only seen in production phase, and the correlation with the metabolic switch indicates that it may as well be related to the lack of the four BGCs or the produced compounds. Further experimental work is needed to determine the causative mechanism for the observed strain difference in ribosomal protein expression.

Reduced production of the polyketide germicidin in M1152

It is a general conception that removal of sinks for valuable precursors improves a strain for heterologous expression, as these metabolites become available for biosynthesis of other compounds. It is therefore remarkable that production of the polyketides germicidin A and B, autologous to both M145 and M1152, are largely reduced in M1152 (**Figure 6E**). Germicidin biosynthesis originates from acyl-carrier proteins intermediate in the fatty acid biosynthesis (99), which are transcriptionally downregulated as a response to the metabolic switch, but while this can prevent an increase of germicidin in M1152, it does not justify the observed 5–20 fold decrease. The reduced growth rate may play a certain role in the observed phenotype but transpires that the BGC deletions and the *rpoB* point mutation have additional, unpredicted consequences in the tightly regulated metabolism of *S. coelicolor* that require further studies to unravel their effects on metabolic function and performance.

Discussion

Normalization affect model predictions

To elucidate the time-dependent behaviours of metabolism in strains with different genetics and corresponding different growth dynamics, we had to compare flux distributions across cells with very different overall metabolic activity. Because of the large difference in uptake and growth rates between both strains and time points, and thus the absolute predicted flux values, normalized data are necessary in order to compare flux distributions. We tested various proxies as indicators of overall metabolic activity for normalization, namely CO_2 production; the total carbon uptake from glucose and glutamate; growth rate and mean flux value. As golden standard, we compared the fluxes through

individual reactions that are well documented to change in M145 in response to the phosphate depletion (**Figure S13**). Normalization based on CO_2 production was selected, but the data normalized on total carbon uptake from glucose and glutamate provided similar results, both for the selected reactions (**Figure S13A and S13B**) and for the pathway analysis (**Figure S14**). The data normalized by the total sum of fluxes shows similar patterns as the glucose/glutamate and CO_2-normalized data but is noisier (**Figure S13C**). For the growth-normalized data, the huge differences in growth rate disguised any other flux patterns (**Figure S13D**). Resultingly, this reassures that the observed differences in metabolic fluxes are not artefacts of the normalization method, but rather corroborated by various indicators of overall metabolic activity.

Genome-scale models provide hypothesis for the growth deficiency of M1152

We have carried out a multi-omics study comparing the metabolism of *Streptomyces coelicolor* M145 and the BGC-deletion mutant M1152 during batch fermentation to understand how these two strains differ in metabolism, both during exponential growth and after phosphate depletion. To enlighten this question from a systems biology perspective, we combined time-course sampled cultivation and transcriptome analysis with enzyme-constrained genome-scale models generated with proteome data to conjecture the mechanisms underlying the phenotypic differences between the two strains. The genome-scale models have been instrumental to allow for direct interpretation on how differences on the transcriptome- and proteome levels propagate to the level of metabolic fluxes. Leveraging metabolic simulations to contextualize transcriptional changes is majorly impacted by the quality of the computational model used. Here, two teams joined efforts to consolidate a consensus model of *S. coelicolor*, resulting in a comprehensive model through open and reproducible development, with an impact beyond this study.

The origin of the reduced growth rate of M1152 remains uncertain, while our results indicate that the growth deficiency can be caused by reduced glucose uptake and the resulting reorganization of central carbon metabolism or by the *rpoB* mutation, possibly in interaction with the BGC deletions. The genome-scale models connect the reduced glucose uptake to increased oxidative stress in M1152, and this is strongly supported by the analysis of differentially expressed genes. According to model predictions this reorganization is accompanied by excretion of metabolites, such that further work including exometabolomic measurements can potentially provide additional model constraints and knowledge. It is intriguing that the M1146 mutant strain in contrast has an increased growth rate compared to M145 (79), as the only difference between these two strains is the *rpoB* single point mutation, which has been shown to enhance antibiotic production without growth impairment in *S. lividans* (22). However, epistatic interactions involving *rpoB* has caused unexpected results in *S. coelicolor* previously (100), and different cultivation conditions when independently comparing strains may contribute to obtaining contradictory results. The defined cultivation media used in this work was chosen because it supports sufficient growth and a delayed, well-defined onset of secondary metabolism, a necessity for studying the metabolic switch (20).

Further development may improve M1152 as host for heterologous expression

It is timely to question the potential of the M1152 strain as a host for heterologous production of secondary metabolites. The strain has several advantages: the removal of the 4 major BGCs not only removes competing sinks for valuable precursors, but the clean background also simplifies the identification of a novel product with mass spectrometry. M1152 has already proved to be more efficient than M145 and M1146 in heterologous production of chloramphenicol and congocidine (13). On the other hand, the reduced growth rate of M1152 can make further development of this strain less favourable compared to e.g. M1146 with its increased growth rate compared to M145 (79).

While previous work suggested a competitive relation between primary and secondary metabolism (101), the ratio between malonyl-CoA consumption into fatty acid biosynthesis and secondary metabolism (**Figure 5**) suggests that the effect of removing the 4 major BGCs on production of heterologous compounds is minor. This corresponds well with the observed increase in heterologous production of chloramphenicol and congocidine, where a 3 to 5-fold increase in production was observed in absence of the 4 major BGCs (strain M1146), while additional rpoB mutation (M1152) yielded 20 to 40-fold increased production (11). This is also in agreement with the results from development of M1317, a strain derived from M1152 by removal of three Type III PKS genes (16): (re-)introduction of germicidin synthase gave a 10.7 and 7.8-fold increase in the total germicidin production for M1317 and M1152, respectively. The rpoB mutation thus has a seemingly much larger impact on the production of secondary metabolites than can be attributed to the increased precursor supply caused by removal of existing sink.

While our modelling efforts are not able to provide a mechanistic explanation for the reported increased production of heterologous compounds in M1152 (11, 16), congocidine and chloramphenicol biosynthesis require additional precursors from the one utilized by Red, Act, CDA and Coelimycin P1. Moreover, differences in cultivation media further convolute cross-study comparisons: the aforementioned studies use a complex growth medium while we used a defined medium with glucose and glutamate, which has previously been optimized for studying the metabolic switch (20). A complete causative understanding of the underlying reasons for the improved production is additionally complicated by the possibility of epistatic interactions between regulatory effects caused by the *rpoB* mutation and removal of gene clusters, and it is inarguable that a comparison including the intermediate strain M1146 (11), or possibly also an M145 strain featuring only the *rpoB* mutation (102), could provide valuable knowledge.

Other approaches for host development may be more efficient. Although *S. coelicolor* seems to have a complex and not fully elucidated regulatory system, several studies have shown that manipulation of regulatory genes can affect production of secondary metabolites (103–106). The complex regulation of secondary metabolite biosynthesis makes rational strain design difficult (107), but black-box approaches including random mutations and screening are still viable approaches for strain development (108, 109). Another approach is to reintroduce *scbR2*, both to avoid influencing the related regulators of development and secondary metabolism and to regain the control of ScbA and production of SCB1, which inhibits Act production (110). Also, morphology plays a major role and the increased growth rate of the non-pelleting *matAB* mutant of *S. coelicolor* may be another starting point for further strain development (111).

Materials and Methods

Sco-GEM consensus model reconstruction and development

A brief description of the model reconstruction process is given in the following section, while all details are described in **Supplemental Information 2.** and in the community model's GitHub repository (https://github.com/SysBioChalmers/sco-GEM). The model is hosted on GitHub to facilitate further development by the community, and we've also created a channel on Gitter dedicated to Sco-GEM questions and discussions (https://gitter.im/SysBioChalmers/Sco-GEM).

Protocol for model merging

Using iKS1317 (15) as a starting point, additional reactions, metabolites and genes were added from Sco4 (37) and iAA1259 (35). These three models are all based on the preceding model iMK1208. To

facilitate model comparison, modified or added reactions and metabolites in Sco4 and iAA1259 were mapped to the iKS1317 namespace by using reaction and metabolite database annotations, reaction equations and metabolite names and formulas. The full list of reactions and metabolites added or modified according to Sco4 and iAA1259 is given in **Tables S6 - S10.**

The next step of the reconstruction process involved mainly manual curations: known flaws and missing gene annotations in iKS1317 and Sco4 were fixed; reactions and metabolites added from Sco4 were given IDs according to the BiGG namespace (56); all reactions, metabolites and genes were given SBO annotations (112) (**Table S11**); all possible reactions and metabolites were given MetaNetX (55) and chebi (54) (metabolites only) annotations; the extensive annotation of genes from iAA1259 were expanded to cover 1591 of the 1777 genes in Sco-GEM. We also created pseudo-metabolites for the redox cofactors NADH/NADPH and NAD+/NADP+ and introduced them into reactions where the cofactor usage is uncertain.

The biomass equation was curated with the following main improvements: 1) Adopting the curation of 2-demethylmenaquinol and menaquinol from iAA1259; 2) Separating the biomass reaction into the pseudometabolites lipid, protein, dna, rna, carbohydrate, cell wall and misc; 3) Updating the coefficients for prosthetic groups based on the proteomics data and information about prosthetic groups for individual proteins from UniProt. Additional details are given in **Supplemental Information 2**.

Model reversibility

By using python-API (https://gitlab.com/elad.noor/equilibrator-api) of eQuilibrator (59) we calculated the change in Gibbs free energy for 770 reactions (**Table S3**). eQuilibrator can only calculate the change in Gibbs free energy for intracellular reactions (i.e. not transport and exchange reactions) where all metabolites are mapped to KEGG (51, 52). The calculations are based on the component contribution method (113). The change in Gibbs free energy was calculated at standard conditions (25 °C, 1 bar), pH7 and 1mM concentration of reactants, denoted $\Delta_r G'^m$ in eQuilibrator. This did not cover any transport or exchange reactions nor reactions with metabolites lacking KEGG annotation. We then applied a threshold of -30 kJ/mol to define a reaction as irreversible (114, 115). Using the set of growth data and knockout data, we evaluated the effect of these changes in reaction reversibility: by randomly applying these changes to 10 reactions at the time we identified single, pair and triplets of reactions that reduced model accuracy when the reversibility was changed based on the change in Gibbs free energy (**Table S12, Supplemental Information 2**).

Analysis and annotation of transport reactions

Gene annotations, substrate and transport class information were mostly extracted from Transport DB 2.0 (116) and TCDB (117). Then, transport proteins were extracted from IUBMB-approved Transporter Classification (TC) System and categorized into 9 main classes (**Figure 1F**): 1) ABC transporter; 2) PTS transporter; 3) Proton symporter; 4) Sodium symporter; 5) Other symporter; 6) Proton antiport; 7) Other antiport; 8) Facilitated diffusion; 9) Simple diffusion. For those transport proteins with an ambiguous substrate annotation in TCDB, the specific substrate annotation was obtain by extracting annotations from KEGG (51, 52), UniProt (57) or through BLAST homology search (118) using a similarity threshold of 90% (see **Supplemental Information 2** and **Table S4** for details).

Development of enzymatically constrained (EcSco-GEM) model

An enzyme-constrained version of the Sco-GEM model (in the following denoted EcSco-GEM) was generated using GECKO (31). The GECKO method enhances an existing GEM by explicitly constraining the maximum flux through each reaction by the maximum capacity of the corresponding enzyme, given by the product of the enzyme abundance and catalytic coefficient. This is facilitated by splitting both

reactions catalysed by isoenzymes and reversible reactions. The Sco-GEM v1.1 model was modified using GECKO version 1.3.4. Kinetic data, in the form of k_{cat} values (s^{-1}), were automatically collected from BRENDA (119). If BRENDA did not report a k_{cat} value for an enzyme, GECKO searched for alternative k_{cat} values by reducing specificity, on the level of substrate, enzymatic activity (EC number) and organism. While 4178 out of 4753 queried enzyme activities could be matched to the full EC code, 306 of the matched activities reported in BRENDA were from *S. coelicolor.* Additionally, six k_{cat} values were manually curated, and a thorough explanation and reasoning behind these modifications are given in the **Supplemental Information 3**. The NAD(H)/NAD(P)H pseudoreactions were blocked to avoid infeasible loops.

Then, separate models were created for each strain (the gene clusters for actinorhodin, undecylprodigiosin, CDA and coelimycin P1 was removed to create M1152) and for each timepoint by using estimated growth, uptake and secretion rates (**Supplemental Information 4**) and proteome measurements. These time point specific models (9 time points for M145, 8 time points for M1152) were used to analyse the activity in individual metabolic pathways through random sampling (65). We also created one EcSco-GEM model for each strain with a global constraint on the protein usage instead of specific protein usage, which were used for model quality control.

Continuous integration and quality control with memote

Validation and quality assessment of Sco-GEM is carried out using the test-suite in memote (42). Memote provides by default a large range of tests, which we have used to identify issues and possible improvements. The test suite reports descriptive model statistics such as the number of genes, reactions and metabolites, and also checks the presence of SBO terms and annotations, the charge and mass balance of all reactions, the network topology and find energy-generating cycles (120). Additionally, we incorporated custom tests into the memote test-suite to automatically compare predicted phenotypes with experimental data in different growth media and for different knockout mutants. The experimental growth and knockout data are extracted from (15). Memote version 0.9.12 was used in this work, and the full memote report for Sco-GEM is given in **Supplemental Information 1**. As a separate evaluation, we applied the method for identifying internal and unrealistic energy-generating cycles by (121) , and no such cycles were found in Sco-GEM.

The simplest use of memote is generating snapshot reports showing the current state of the model. However, by integrating Travis CI [https://travis-ci.com/] into the gitHub repository, memote can be used to create a continuous report displaying how each commit affects the model quality.

Random sampling, normalization and pathway analysis

Because of the huge number of reactions in the EcSco-GEM, it is challenging to sample the solution space appropriately: we have chosen to use the method provided in the Raven Toolbox 2 (37, 65) which sample the vertices of the solution space. The drawback of this method is that it will not result in a uniform sampling of the solution space. However, it is more likely to span the entire solution space and also not prone to get stuck in extremely narrow parts of the solution space, which may happen with variants of the hit-and-run algorithm (122–124). For each of the time points for each strain (17 different conditions in total) we generated 5000 random flux distributions with Gurobi as the solver. The reactions catalysed by isoenzymes were combined into the set of reactions in Sco-GEM and the reactions providing protein for each reaction. The mean of the 5000 flux distributions for each metabolic reaction was used in the following analysis. For each of the 17 conditions, the mean fluxes were normalized by the CO_2 production rate. Then, the normalized mean fluxes were summarized for each metabolic pathway by using the curated pathway annotations, and we consider this a measure of the metabolic activity in each pathway.

Strains, cultivation conditions, sampling procedures, and analyses of media components and antibiotics box

Experiments were performed using strain M145 of *S. coelicolor* A3(2) and its derivative M1152, lacking the 4 major BGCs for actinorhodin (Act), undecylprodigiosin (Red), coelimycin P1 (Cpk), and calcium-dependent antibiotic (CDA), and carrying the pleiotropic, previously described antibiotic production enhancing mutation *rpoB* [S433L] (13, 22). Both strains were kindly provided by Mervyn Bibb at John-Innes-Centre, Norwich, UK.

Triplicate cultivations of the strains were performed based on germinated spore inoculum on 1.8 L phosphate-limited medium SSBM-P, applying all routines of the optimized submerged batch fermentation strategy for *S. coelicolor* established and described before (20). All media were based on ion-free water, and all chemicals used were of analytical grade. In brief, spore batches of M145 and M1152 were generated by cultivation on soy flour-mannitol (SFM) agar plates (125), harvesting by scraping of spores and suspension in 20% (v/v) glycerol, and storage in aliquots at −80 °C. 10^9 CFU of spores of each strain were germinated for 5 hours at 30 °C and 250 rpm in 250 mL baffled shake-flasks with 2 g of 3 mm glass beads and 50 mL 2x YT medium (126). The germinated spores were harvested by centrifugation (3200 x g, 15 °C, 5 min) and re-suspended in 5 mL ion-free water. An even dispersion of the germinated spores was achieved by vortex mixing (30 s), ensuring comparable inocula among biological replicas. Each bioreactor (1.8 liter starting volume culture medium in 3-liter Applikon stirred tank reactors) was inoculated with 4.5 mL germinated spore suspension (corresponding to $9x10^8$ CFU). Phosphate-limited medium SSBM-P (8) consisted of Na-glutamate, 55.2 g/L; D-glucose, 40 g/L; $MgSO_4$, 2.0 mM; phosphate, 4.6 mM; supplemented minimal medium trace element solution SMM-TE (126), 8 mL/L and TMS1, 5.6 mL/L. TMS1 consisted of $FeSO_4$ x 7 H_2O, 5 g/L; $CuSO_4$ x 5 H_2O, 390 mg/L; $ZnSO_4$ x 7 H_2O, 440 mg/L; $MnSO_4$ x H_2O, 150 mg/L; Na_2MoO_4 x 2 H_2O, 10 mg/L; $CoCl_2$ x 6 H_2O, 20 mg/L, and HCl, 50 mL/L. Clerol FBA 622 fermentation defoamer (Diamond Shamrock Scandinavia) was added to the growth medium before inoculation. Throughout fermentations, pH 7.0 was maintained constant by automatic addition of 2 M HCl. Dissolved oxygen levels were maintained at a minimum of 50% by automatic adjustment of the stirrer speed (minimal agitation 325 rpm). The aeration rate was constant 0.5 L/(L x min) sterile air. Dissolved oxygen, agitation speed and carbon dioxide evolution rate were measured and logged on-line, while samples for the determination of cell dry weight, levels of growth medium components and secondary metabolites concentrations, as well as for transcriptome and proteome analysis were withdrawn throughout the fermentation trials as indicated in **Figure 2B**. For transcriptome analysis, 3 × 4 ml culture sample were applied in parallel onto three 0.45 µm nitrocellulose filters (Millipore) connected to vacuum. The biomass on each filter was immediately washed twice with 4 ml double-autoclaved ion-free water pre-heated to 30 °C, before the filters were collected in a 50 ml plastic tube, frozen in liquid nitrogen and stored at -80 °C until RNA isolation. For proteome analysis, 5 ml samples were taken and centrifuged (3200 x g, 5 min, 4 °C), and the resulting cell pellets frozen rapidly at -80 °C until further processing.

Levels of phosphate were measured spectrophotometrically by using the SpectroQuant Phosphate test kit (Merck KGaA, Darmstadt, Germany) following the manufacturer's instructions after downscaling to 96-well plate format. D-glucose and L-glutamate concentrations were determined by LC-MS using suitable standards, and measured concentrations were used to estimate specific uptake and excretion rates. Undecylprodigiosin (RED) levels were determined spectrophotometrically at 530 nm after acidified methanol extraction from the mycelium (127). To determine relative amounts of actinorhodins (determined as total blue pigments, TBP), cell culture samples were treated with KOH (final concentration 1 M) and centrifuged, and the absorbance of the supernatants at 640 nm was determined (127). Quantification of germicidin A and B was performed using targeted LC-MS analytics.

Proteomics

Sample preparation and NanoUPLC-MS analysis

Mycelium pellets for proteome analysis were thawed and resuspended in the remaining liquid. 50 µL re-suspended mycelium was withdrawn and pelleted by centrifugation. 100 µL lysis buffer (4% SDS, 100 mM Tris-HCl pH 7.6, 50 mM EDTA) was added, and samples were sonicated in a water bath sonicator (Biorupter Plus, Diagenode) for 5 cycles of 30 s high power and 30 s off in ice water. Cell debris was pelleted and removed by centrifugation. Total protein was precipitated using the chloroform-methanol method described before (128). The pellet was dried in a vacuum centrifuge before dissolving in 0.1% RapiGest SF surfactant (Waters) at 95 °C. The protein concentration was measured at this stage using BCA method. Protein samples were then reduced by adding 5 mM DTT, followed by alkylation using 21.6 mM iodoacetamide. Then trypsin (recombinant, proteomics grade, Roche) was added at 0.1 µg per 10 µg protein. Samples were digested at 37 °C overnight. After digestion, trifluoroacetic acid was added to 0.5% followed by incubation at 37 °C for 30 min and centrifugation to remove MS interfering part of RapiGest SF. Peptide solution containing 8 µg peptide was then cleaned and desalted using STAGE-Tipping technique (129). Final peptide concentration was adjusted to 40 ng/µL using sample solution (3% acetonitrile, 0.5% formic acid) for analysis.

200 ng (5 µL) digested peptide was injected and analysed by reversed-phase liquid chromatography on a nanoAcquity UPLC system (Waters) equipped with HSS-T3 C18 1.8 µm, 75 µm X 250 mm column (Waters). A gradient from 1% to 40% acetonitrile in 110 min (ending with a brief regeneration step to 90% for 3 min) was applied. [Glu^1]-fibrinopeptide B was used as lock mass compound and sampled every 30 s. Online MS/MS analysis was done using Synapt G2-Si HDMS mass spectrometer (Waters) with an $UDMS^E$ method set up as described in (130).

Data processing and label-free quantification

Raw data from all samples were first analysed using the vender software ProteinLynx Global SERVER (PLGS) version 3.0.3. Generally, mass spectrum data were generated using an MS^E processing parameter with charge 2 lock mass 785.8426, and default energy thresholds. For protein identification, default workflow parameters except an additional acetyl in N-terminal variable modification were used. Reference protein database was downloaded from GenBank with the accession number NC_003888.3. The resulted dataset was imported to ISOQuant version 1.8 (130) for label-free quantification. Default high identification parameters were used in the quantification process. TOP3 result was converted to PPM (protein weight) and send to the modelers and others involved in interpreting the data (**Table S13**).

TOP3 quantification was filtered to remove identifications meet these two criteria: 1. identified in lower than 70% of samples of each strain and 2. sum of TOP3 value less than 1×10^5. Cleaned quantification data was further subjected to DESeq2 package version 1.22.2 (29) and PCA was conducted after variance stabilizing transformation (vst) of normalized data.

Transcriptomics

RNA extraction and quality control

Bacteria were lysed using RNAprotect Bacteria (Qiagen) and following the manufacturer´s instruction. Briefly, filters containing bacteria were incubated with 4 ml of RNAprotect Bacteria Reagent. After centrifugation, resulting samples were lysed using 500 µl of TE buffer (10 mM Tris·Cl, 1 mM EDTA, pH 8.0) containing 15 mg/ml lysozyme using 150-600 µm diameter glass beads (Sigma) agitated at 30 Hz for 5 minutes in the TissueLyser II (Qiagen).

Total RNA was extracted using RNeasy mini kit (Qiagen) and 700 µl of the resulting lysate complemented with 470 µl of absolute ethanol. RNAase-free DNase set (Qiagen) and centrifugation steps were performed to prevent DNA and ethanol contamination. Elution was performed using 30 µl of RNase-free water and by reloading the eluate on the column to improve the RNA yield. The RNA concentration was measured using Qubit RNA BR Assay Kit (ThermoFisher Scientific), RNA purity was assessed using A260/A280 and A260/A230 ratio using the Nano Drop ND-1000 Spectrophotometer (PEQLAB). RNA Integrity Number was estimated using RNA 6000 Nano Kit (Agilent) and the Bioanalyzer 2100 (Agilent).

Library preparation and sequencing

A total of 1 µg of total RNA was subjected to rRNA depletion using Ribo-Zero rRNA Removal Kit Bacteria (Illumina). The cDNA libraries were constructed using the resulting tRNA and the NEBNext Ultra II Directional RNA Library Prep Kit (NEB). Libraries were sequenced as single-reads (75 bp read length) on an Illumina NextSeq500 platform at a depth of 8–10 million reads each.

RNA-seq data assessment and analysis

Sequencing statistics including the quality per base and adapter content assessment of resulting transcriptome sequencing data were conducted with FastQC v0.11.5 (131). All reads mappings were performed against the reference strain of *Streptomyces coelicolor A3(2)* (RefSeq ID NC_003888.3). The mappings of all samples were conducted with HISAT2 v2.1.0 (132). As parameters, spliced alignment of reads was disabled, and strand-specific information was set to reverse complemented (HISAT2 parameter --no-spliced-alignment and --rna-strandness "R"). The resulting mapping files in SAM format were converted to BAM format using SAMtools v1.6 (133). Mapping statistics, including strand specificity estimation, percentage of mapped reads and fraction exonic region coverage, were conducted with the RNA-seq module of QualiMap2 v2.2.2-dev (134). Gene counts for all samples were computed with featureCounts v1.6.0 (28) based on the annotation of the respective reference genome, where the selected feature type was set to transcript records (featureCounts parameter -t transcript).

To assess variability of the replicates of each time series, a principal component analysis (PCA) was conducted with the DESeq2 package v1.20.0, see **Figure S15** (29).

Normalization and differential gene expression

Raw count files were imported into Mayday SeaSight (135) for common, time-series-wide normalization. For this, the raw counts of all biological replicates of one strain across the time-series were log2-transformed (with pseudocount of +1 for the genes with zero counts) and then quantile-normalized. To make the two normalized time-series data of M154 and M1152 comparable, they were again quantile-normalized against each other. The normalized RNA-seq data are provided in **Table S14.**

Differentially expressed genes were identified by ANOVA using Orange (v3.2) and the bioinformatic toolkit (v), with FDR of <0.01 and a minimal fold enrichment >1 for at least one aligned timepoint. Genes with low expression (log2 < 5 for both strains and timepoints) were not considered for further analysis. The differentially expressed genes were subsequently scaled to the expression average and clustered by K-means. Visualization of genes and clusters were performed in python (v3.7) with matplotlib (v3.1.1). For this, the time-series of M145 and M1152 were aligned such that in the visual representation, the expression profiles of the two strains are aligned relative to the time point of phosphate depletion. Both DAVID (136, 137) and the string database (138) was used to evaluate the function of each cluster, identifying overrepresentation of function groups based on GO annotation or text mining. Identified differential clusters or regulons were extracted from literature and plotted (**Table S15, Figure S8 and S9**).

Data and Software Availability

Model repository

The model is hosted and developed in an open repository on GitHub: https://github.com/SysBioChalmers/Sco-GEM. Here, the latest version of the Sco-GEM is available in both YAML and SBML level 3 Version 1. Additionally, users can see all details of the model reconstruction and contribute to further model development by posting issues or suggest changes. This should encourage further, incremental development of Sco-GEM by the community.

Proteome data

The proteomics data have been deposited to the ProteomeXchange Consortium via the PRIDE (139) partner repository with the dataset identifier PXD013178 and 10.6019/PXD013178. Normalized proteome data is also available in **Table S13.**

Transcriptomics data

All high-throughput sequencing data have been deposited in NCBI's Gene Expression Omnibus and are accessible under accession number GSE132487 (M145) and GSE132488 (M1152). Normalized counts are also found in **Table S14.**

Author contributions

Conceptualization, E.K., E.A., A.W., S.S., A.S.Y. and T.K. Methodology and software, E.K., S.S., A.S.Y. and T.K. Validation and formal analysis, C.D., K.N., D.V.D., S.S., T.K., E.K. Investigation, T.K., A.W., S.S., E.K. Data curation, S.S., T.K. Writing - original draft, S.S., T.K., D.V.D., C.D., K.N. Writing – review & editing, all authors. Visualization, S.S., E.K., C.D., D.V.D. Supervision, A.W., E.A., E.K. Project administration, A.W. Funding acquisition: A.W., E.K., E.A.

Acknowledgements

The authors would like to acknowledge Bogdan I. Florea of Leiden University, Leiden, Netherlands, for running and monitoring the proteome measurements, and the bio-organic synthesis group at Leiden University for providing the opportunity to use their instrumentation. The authors would also like to acknowledge co-workers at SINTEF Industry, Trondheim, Norway: Ingemar Nærdal, Anna Lewin and Kari Hjelen for running the batch fermentations and Anna Nordborg, Janne Beate Øiaas and Tone Haugen for performing offline analyses and the germicidin analytics. The RNA-Seq sequencing was carried out by c.ATG, Tübingen, Germany.

Finally, the authors would also like to acknowledge Gilles van Wezel, Olaf Wolkenhauer, Håvard Sletta and Trond E. Ellingsen for contributing in the development of the concept and structure of this work. Håvard Sletta and Olaf Wolkenhauer also contributed by proofreading the manuscript.

This study was conducted in the frame of ERA-net for Applied Systems Biology (ERA-SysAPP) project SYSTERACT and the project INBioPharm of the Centre for Digital Live Norway (Research Council of Norway grant no. 248885). The authors declare no conflict of interest.

Supplemental Information

1. Memote snapshot report of Sco-GEM
2. Protocol for Sco-GEM model development
3. Details of EcSco-GEM development

4. Estimation of growth rates, uptake rates and secretion rates for M145 and M1152 based on online and offline measurements

Figures

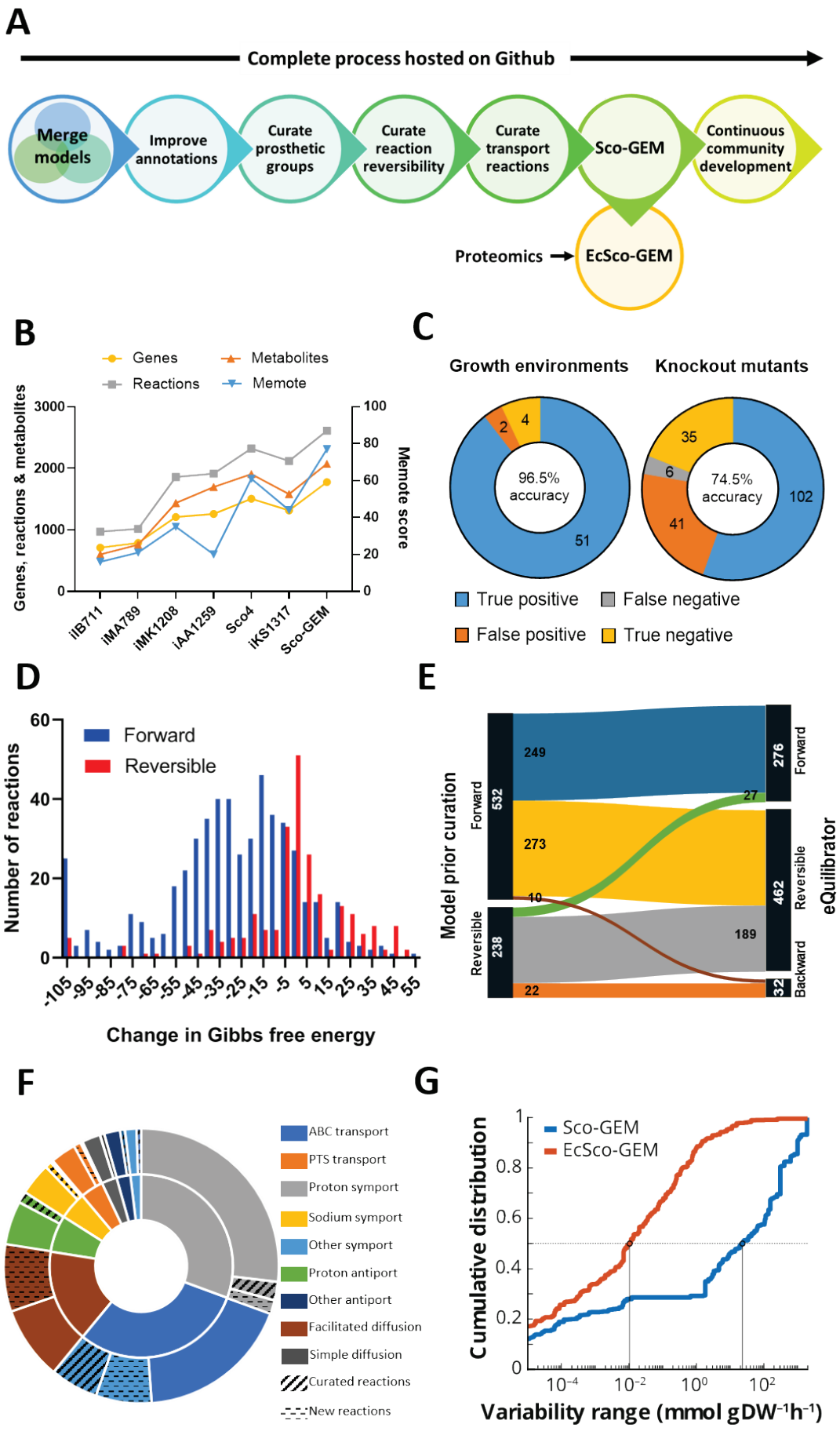

Figure 1: Sco-GEM development and analysis. *A) The Sco-GEM model is reconstructed by merging iAA1259, Sco4 and iKS1317. The model is further developed by improving annotations and curating the coefficients for prosthetic groups in the biomass function reaction reversibility and transport reactions. An enzyme-constrained model is generated from Sco-GEM by incorporating catalytic constants and proteomics data. The complete development is hosted as a public repository on GitHub, allowing detailed insight and further development by the community. B) The overall memote score and the number of genes, reactions and metabolites for the 7 published genome-scale metabolic model of S. coelicolor. C) In total 369 transport reactions included in Sco-GEM, whereof 42 were curated and 65 added during this work. The inner ring categorizes the reactions into 9 different subgroups, while the outer ring displays the amount of curated and added reactions within each category. D) The change in Gibbs free energy for 770 reactions, separated into reversible (red) and forward irreversible (blue) based on the assigned bounds in the model before curation. The histogram is truncated at -105 kJ/mol, and more negative values are assigned to the leftmost bin. The graph without truncation is given in* ***Figure S1****. E) Analysis and comparison of the direction of the model reactions before curation and the direction inferred from the change in Gibbs free energy. F) Assessment of the model quality by comparing in vivo observations with in silico predictions: 96.5% accuracy (55/57) for different growth environments and 76.1% accuracy (134/176) different knockout mutants. G) By comparing the cumulative flux variability distribution for Sco-GEM and EcSco-GEM we observe that the incorporation of kinetic coefficients in EcSco-GEM greatly constrains the solution space.*

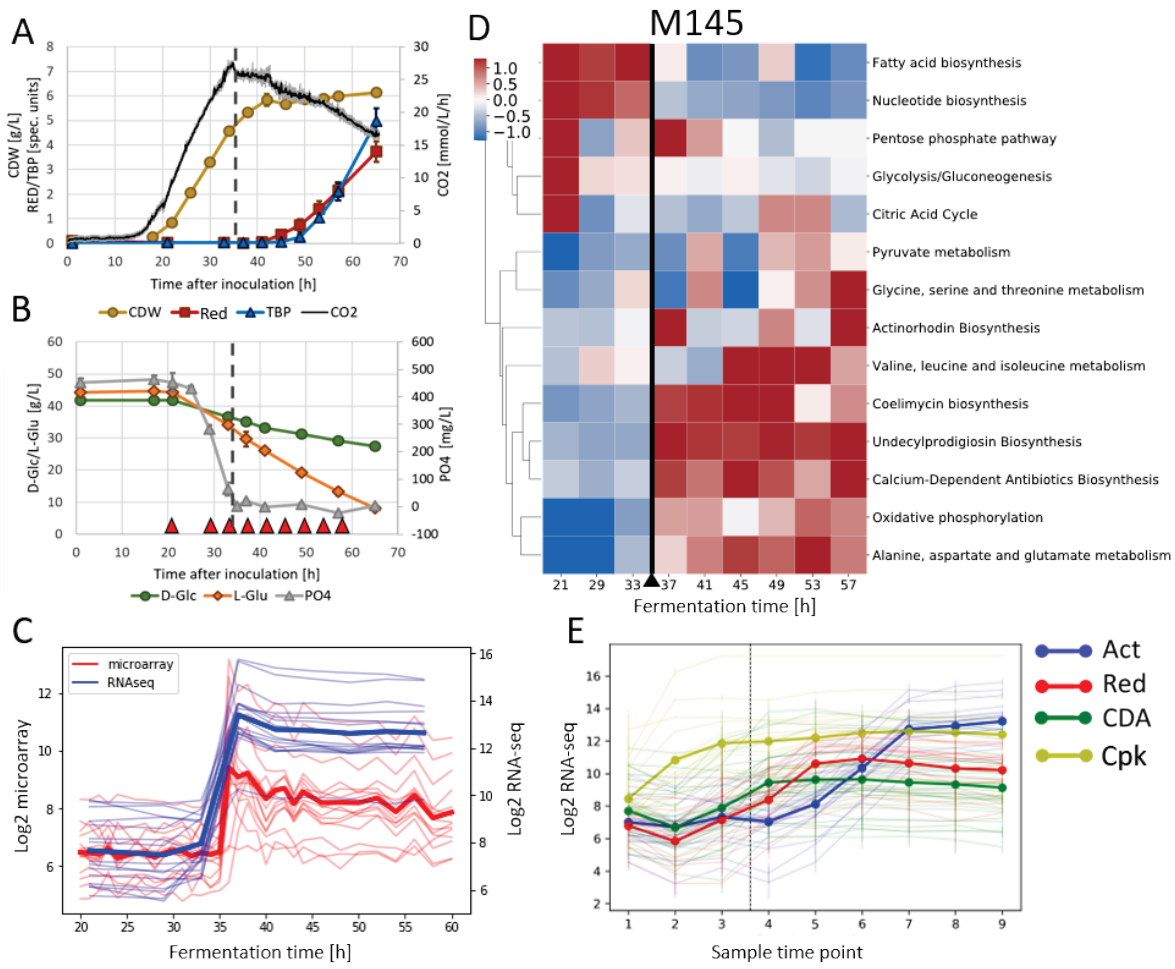

Figure 2: Batch cultivation of S. coelicolor M145 and the effect of phosphate depletion. *Compounds produced (A) and consumed (B) during batch fermentation of S. coelicolor M145. Time points for sampling for transcriptome and proteome analysis are indicated with red upward triangles. The dashed vertical line indicates the time when phosphate in the medium has been depleted. Error bars represent standard deviations of measurement data of three biological replicas. CDW, Cell Dry Weight; Red, undecylprodigiosin; TBP, Total Blue Pigments/actinorhodins; CO2, volume corrected respiration; D-Glc, D-glucose; L-Glu, L-glutamate; PO4, phosphate. C) Good agreement between microarray data (red) (8) and RNA-seq data (blue; this study) for the genes previously found to respond to phosphate depletion (8). D) By incorporating the proteomics data derived from the sample series into the developed genome-scale model we get additional insight into changes in metabolism during the time-course of the cultivation. The clustered heatmap shows CO_2-normalized Z-scores for each of the top 10 varying pathways plus the pathways for the 4 major BGCs in M145 as revealed by EcSco-GEM.* The black vertical line indicates the time point of the metabolic switch. *E) RNA-seq data of the 4 major BGCs show the onset of biosynthesis of actinorhodin (Act),*

undecylprodigiosin (Red), calcium-dependent antibiotic (CDA) and coelimycin (Cpk) at different time points during the batch fermentations of M145.

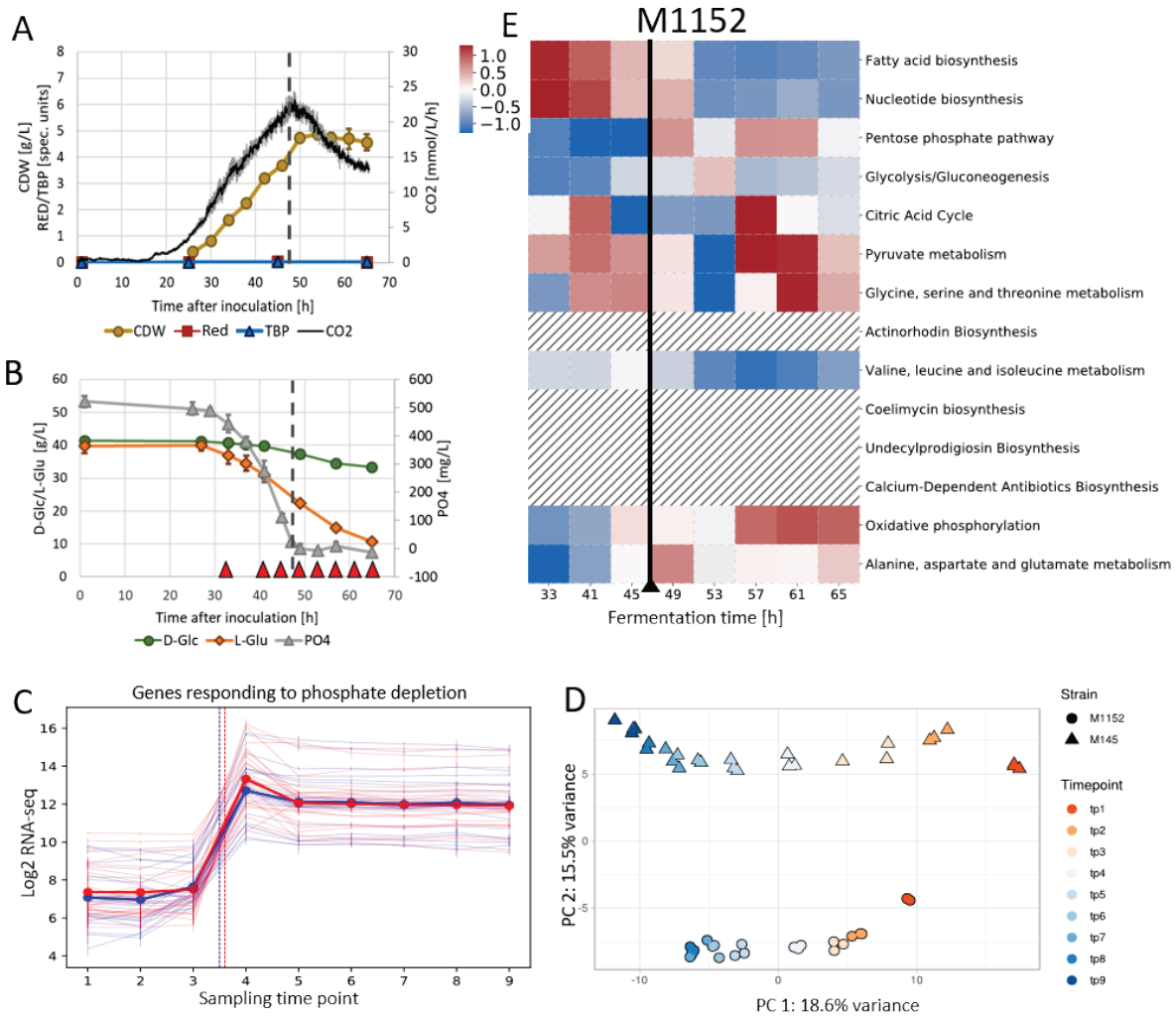

Figure 3: Batch cultivation of M1152. *Compounds produced (A) and consumed (B) during batch fermentation of S. coelicolor M1152. Time points for sampling for transcriptome and proteome analysis are indicated with red upward arrows. The dashed vertical line indicates the time when phosphate in the medium has been depleted. Error bars represent standard deviation of measurement data of three biological replicas. CDW, Cell Dry Weight; Red, undecylprodigiosin; TBP, Total Blue Pigments/actinorhodins; CO2, volume corrected respiration; D-Glc, D-glucose; L-Glu, L-glutamate; PO4, phosphate. C) The genes that were found earlier to respond to phosphate depletion by Nieselt et al., 2010 (8), were used to align the different samples for M145 (blue) or M1152 (red) in respect to the metabolic switch. Shown is the average of all RNA reads with error bars representing the standard deviation between triplicate cultivations. The mean of the entire regulated cluster is given in bold. Vertical dashed lines represent the time points of phosphate depletion for the respective strains. D) PCA-plot of the proteomics data for M145 (triangles) and M1152 (circles), for each time-point and culture. The first principal component separates the time points while the second principal component separates the two strains. E) CO2-normalized Z-scores of pathway fluxes predicted by EcSco-GEM for 10 of the most varying pathways in M145 and M1152. The data for M145 (**Figure 2D**) and M1152 are standardized together to make values and colours comparable. Hatched squares mark the pathways encoded by the four gene clusters removed from M1152.*

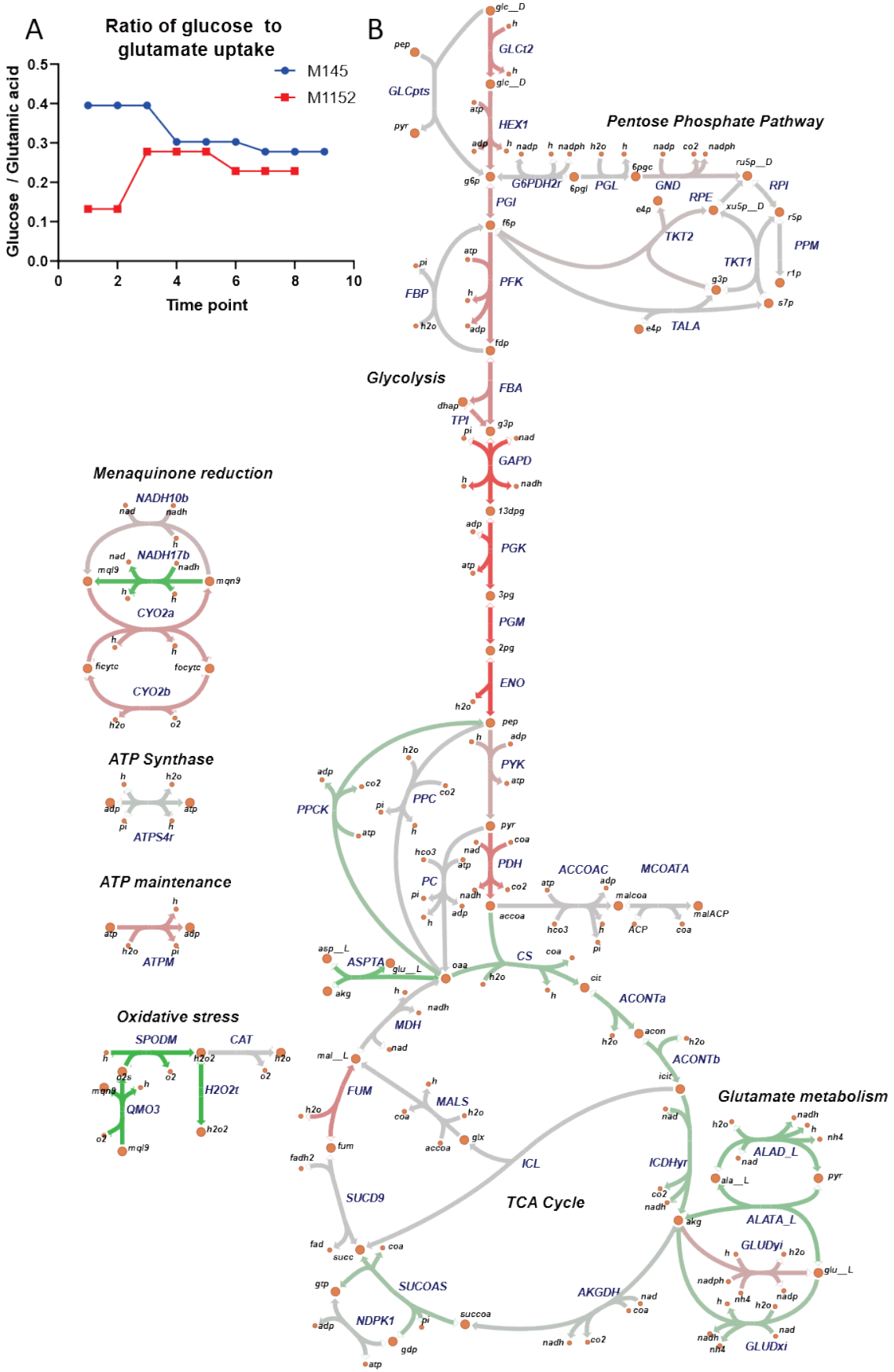

Figure 4: Predicted carbon fluxes in M145 and M1152. *A) The ratio between estimated uptake rates of glucose and glutamate shows that M1152 acquires a smaller part of its carbon from glucose compared to M145. The difference is most notable during growth phase, represented by the first timepoints. B) By comparing the predicted fluxes for the second sampling time points for M145 and M1152, i.e. after 29 and 41 hours, respectively, differences in metabolism between the two strains are clearly observable and how these connect to the reduced biomass-specific uptake rate of glucose in M1152. The second time point for each strain was chosen because the estimated uptake rates are more reliable than the first time point. The strength of the colour of the lines correspond to the flux difference between the strains; green reactions have higher flux in M1152, and red reactions have higher flux in M145.*

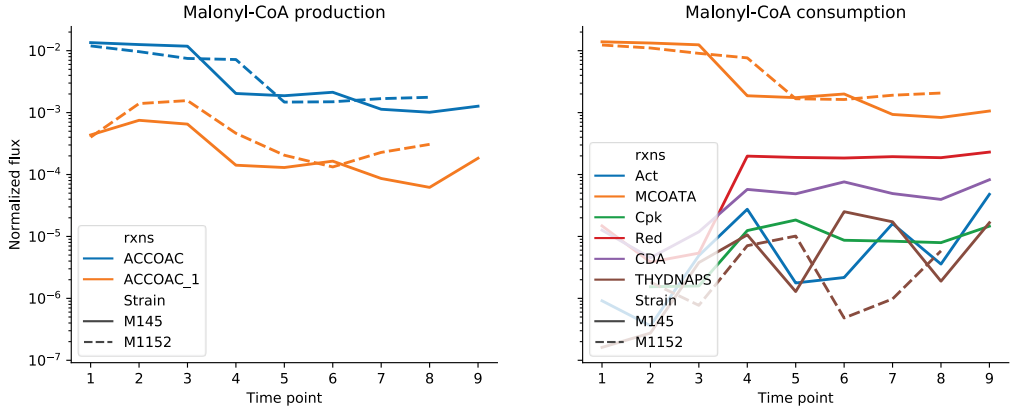

Figure 5: Production and consumption of malonyl-CoA is the branching point between fatty acid biosynthesis and production of polyketides*. From EcSco-GEM predictions, we observe a clear downregulation of the malonyl-CoA production (left panel) by both acetyl-CoA carboxylase (ACCOAT; blue) and acetyl-CoA carboxytransferase (ACCOAT_1; orange) in both strains, but the process is clearly delayed and slower in M1152. In the right panel, we observe that most of the malonyl-CoA is directed to fatty acid biosynthesis through malonyl-CoA-ACP transacylase (MCOATA), even after metabolic switching, and that this consumption balances the malonyl-CoA production. The other main sinks for Malonyl-CoA are the pathways encoded by the 4 major BGCs (Act, Cpk, Red and CDA)* in addition to biflaviolin synthase (THYDNAPS).

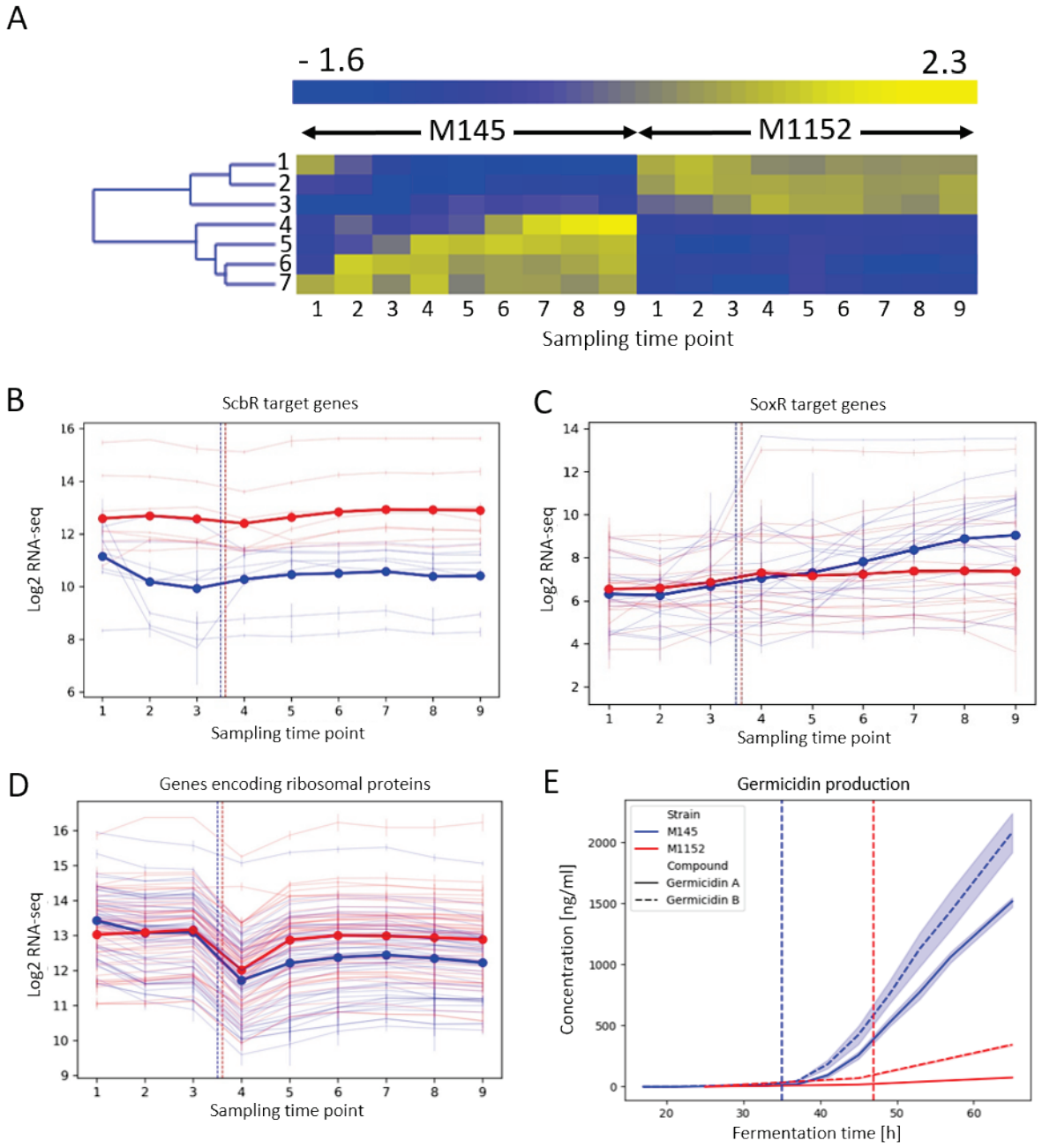

Figure 4: Analysis of transcriptome data and germicidin production. *A) Unsupervised clustering (K-Means) of significantly changed genes into 7 clusters: The first three (clusters 1-3) are upregulated in M1152, while the last four (clusters 4-7) are upregulated from the beginning or at later time points in M145. B) One striking difference in M1152 is the significantly higher expression of genes of the ScbR regulon at all time points analysed, including scbA and scbC. C) From the RNA-seq data, we find a 2-fold reduction in the SoxR regulon at later time points for M1152 (red) compared to M145 (blue). D) From the RNA-seq data we find that the transcription of ribosomal protein genes is increased after the metabolic switch in M1152 (red) compared to (M145 (blue). E) Measured concentrations of germicidin A and B for M1152 and M145. The shaded regions display the uncertainty range based on three replicate cultivations. After phosphate depletion at 35 and 47 hours for M145 and M1152, respectively (vertical lines), M145 produces germicidin at a much higher rate than M1152.*

References

1. Hopwood, David A. 2007. Streptomyces in nature and medicine: the antibiotic makers. Oxford University Press, USA.

2. Hahn J-S, Oh S-Y, Roe J-H. 2002. Role of OxyR as a Peroxide-Sensing Positive Regulator in Streptomyces coelicolor A3(2). Journal of Bacteriology 184:5214–5222.

3. Hutchings MI, Hoskisson PA, Chandra G, Buttner MJ. 2004. Sensing and responding to diverse extracellular signals? Analysis of the sensor kinases and response regulators of Streptomyces coelicolor A3(2). Microbiology, 150:2795–2806.

4. Nothaft H, Rigali S, Boomsma B, Swiatek M, McDowall KJ, Wezel GPV, Titgemeyer F. 2010. The permease gene nagE2 is the key to N-acetylglucosamine sensing and utilization in Streptomyces coelicolor and is subject to multi-level control. Molecular Microbiology 75:1133–1144.

5. Rigali S, Titgemeyer F, Barends S, Mulder S, Thomae AW, Hopwood DA, van Wezel GP. 2008. Feast or famine: the global regulator DasR links nutrient stress to antibiotic production by Streptomyces. EMBO reports 9:670–675.

6. Sola-Landa A, Rodríguez-García A, Franco-Domínguez E, Martín JF. 2005. Binding of PhoP to promoters of phosphate-regulated genes in Streptomyces coelicolor: identification of PHO boxes. Molecular Microbiology 56:1373–1385.

7. Chandra G, Chater KF. 2014. Developmental biology of Streptomyces from the perspective of 100 actinobacterial genome sequences. FEMS Microbiol Rev 38:345–379.

8. Nieselt K, Battke F, Herbig A, Bruheim P, Wentzel A, Jakobsen ØM, Sletta H, Alam MT, Merlo ME, Moore J, Omara WA, Morrissey ER, Juarez-Hermosillo MA, Rodríguez-García A, Nentwich M, Thomas L, Iqbal M, Legaie R, Gaze WH, Challis GL, Jansen RC, Dijkhuizen L, Rand DA, Wild DL, Bonin M, Reuther J, Wohlleben W, Smith MC, Burroughs NJ, Martín JF, Hodgson DA, Takano E,

Breitling R, Ellingsen TE, Wellington EM, Kolter R, Siegele D, Tormo A, Hesketh A, Bucca G, Laing E, Flett F, Hotchkiss G, Smith C, Chater K, Hesketh A, Chen W, Ryding J, Chang S, Bibb M, Huang J, Lih C, Pan K, Cohen S, Lian W, Jayapal K, Charaniya S, Mehra S, Glod F, Kyung Y, Sherman D, Hu W, Strauch E, Takano E, Baylis H, Bibb M, DeRisi J, Iyer V, Brown P, Reuther J, Wohlleben W, Fink D, Weissschuh N, Reuther J, Wohlleben W, Engels A, Tiffert Y, Supra P, Wurm R, Wohlleben W, Wagner R, Reuther J, Pawlik K, Kotowska M, Chater K, Kuczek K, Takano E, Takano E, Chakraburtty R, Nihira T, Yamada Y, Bibb M, Takano E, Kinoshita H, Mersinias V, Bucca G, Hotchkiss G, Nihira T, Smith C, Bibb M, Wohlleben W, Chater K, Kotowska M, Pawlik K, Smulczyk-Krawczyszyn A, Bartosz-Bechowski H, Kuczek K, Claessen D, Rink R, Jong W de, Siebring J, Vreugd P de, Boersma F, Dijkhuizen L, Wosten H, Bibb M, Molle V, Buttner M, Ryding N, Kelemen G, Whatling C, Flardh K, Buttner M, Chater K, Ohnishi Y, Seo J, Horinouchi S, Sola-Landa A, Moura R, Martín J, Sola-Landa A, Rodríguez-García A, Franco-Domínguez E, Martín J, Rodríguez-García A, Barreiro C, Santos-Beneit F, Sola-Landa A, Martín J, Sola-Landa A, Rodríguez-García A, Apel A, Martín J, Feitelson J, Malpartida F, Hopwood D, Hallam S, Malpartida F, Hopwood D, Takano E, Gramajo H, Strauch E, Andres N, White J, Bibb M, Kieser T, Bibb M, Buttner M, Chater K, Hopwood D, Bystrykh L, Fernandez-Moreno M, Herrema J, Malpartida F, Hopwood D, Dijkhuizen L, Irizarry R, Bolstad B, Collin F, Cope L, Hobbs B, Speed T, Ihaka R, Gentleman R, Dietzsch J, Gehlenborg N, Nieselt K. 2010. The dynamic architecture of the metabolic switch in Streptomyces coelicolor. BMC Genomics 11:10.

9. Thomas L, Hodgson DA, Wentzel A, Nieselt K, Ellingsen TE, Moore J, Morrissey ER, Legaie R, STREAM Consortium TS, Wohlleben W, Rodríguez-García A, Martín JF, Burroughs NJ, Wellington EMH, Smith MCM. 2012. Metabolic switches and adaptations deduced from the proteomes of Streptomyces coelicolor wild type and phoP mutant grown in batch culture. Molecular & cellular proteomics : MCP 11:M111.013797.

10. Bentley SD, Chater KF, Cerdeño-Tárraga A-MA-M, Challis GL, Thomson NR, James KD, Harris DE, Quail MA, Kieser H, Harper D, Bateman A, Brown S, Chandra G, Chen CW, Collins M, Cronin A, Fraser A, Goble A, Hidalgo J, Hornsby T, Howarth S, Huang C-HC-H, Kieser T, Larke L, Murphy L, Oliver K, O'Neil S, Rabbinowitsch E, Rajandream MM-A, Rutherford K, Rutter S, Seeger K, Saunders D, Sharp S, Squares R, Squares S, Taylor K, Warren T, Wietzorrek A, Woodward J, Barrell BG, Parkhill J, Hopwood DA. 2002. Complete genome sequence of the model actinomycete Streptomyces coelicolor A3(2). Nature 417:141–147.

11. Gomez-Escribano JP, Song L, Fox DJ, Yeo V, Bibb MJ, Challis GL. 2012. Structure and biosynthesis of the unusual polyketide alkaloid coelimycin P1, a metabolic product of the cpk gene cluster of Streptomyces coelicolor M145. Chem Sci 3:2716–2720.

12. Castro JF, Razmilic V, Gomez-Escribano JP, Andrews B, Asenjo JA, Bibb MJ. 2015. Identification and Heterologous Expression of the Chaxamycin Biosynthesis Gene Cluster from Streptomyces leeuwenhoekii. Appl Environ Microbiol 81:5820–5831.

13. Gomez-Escribano JP, Bibb MJ. 2011. Engineering Streptomyces coelicolor for heterologous expression of secondary metabolite gene clusters. Microbial Biotechnology 4:207–215.

14. Gomez-Escribano JP, Bibb MJ. 2014. Heterologous expression of natural product biosynthetic gene clusters in Streptomyces coelicolor: from genome mining to manipulation of biosynthetic pathways. Journal of Industrial Microbiology & Biotechnology 41:425–431.

15. Kumelj T, Sulheim S, Wentzel A, Almaas E. 2018. Predicting Strain Engineering Strategies Using iKS1317: A Genome-Scale Metabolic Model of Streptomyces coelicolor. Biotechnology Journal 0:1800180.

16. Thanapipatsiri A, Claesen J, Gomez-Escribano J-P, Bibb M, Thamchaipenet A. 2015. A Streptomyces coelicolor host for the heterologous expression of Type III polyketide synthase genes. Microb Cell Fact 14.

17. Yin J, Hoffmann M, Bian X, Tu Q, Yan F, Xia L, Ding X, Francis Stewart A, Müller R, Fu J, Zhang Y. 2015. Direct cloning and heterologous expression of the salinomycin biosynthetic gene cluster from Streptomyces albus DSM41398 in Streptomyces coelicolor A3(2). Scientific Reports 5:15081.

18. Nepal KK, Wang G. 2019. Streptomycetes: Surrogate hosts for the genetic manipulation of biosynthetic gene clusters and production of natural products. Biotechnology Advances 37:1–20.

19. Rutledge PJ, Challis GL. 2015. Discovery of microbial natural products by activation of silent biosynthetic gene clusters. Nature Reviews Microbiology 13:509–523.

20. Wentzel A, Bruheim P, Øverby A, Jakobsen ØM, Sletta H, Omara WAM, Hodgson DA, Ellingsen TE, Hopwood D, Bentley S, Chater K, Cerdeno-Tarraga A, Challis G, Thomson N, James K, Harris D, Quail M, Kieser H, Harper D, Klieneberger-Nobel E, Chater K, Hopwood D, Chater K, Bibb M, Lakey J, Lea E, Rudd B, Wright H, Hopwood D, Wright L, Hopwood D, Feitelson J, Hopwood D, Bibb M, Rokem J, Lantz S, Eliasson A, Nielsen J, Song S, Jeong Y, Kim P, Chun G, Rosa J, Neto AB, Hokka C, Badino A, Kieser T, Bibb M, Buttner M, Chater K, Hopwood D, Hayes A, Hobbs G, Smith C, Oliver S, Butler P, Evans C, Herbet D, Tempest D, Takano E, Gramajo H, Strauch E, Andres N, White J, Bibb M, Bruheim P, Sletta H, Bibb M, White J, Levine D, Hodgson D, Nieselt K, Battke F, Herbig A, Bruheim P, Wentzel A, Jakobsen O, Sletta H, Alam M, Merlo M, Moore J, Alam M, Merlo M, Hodgson D, Wellington E, Takano E, Breitling R, Battke F, Symons S, Nieselt K, Battke F, Herbig A, Wentzel A, Jakobsen O, Bonin M, Hodgson D, Wohlleben W, Ellingsen T, Nieselt K, Thomas L, Hodgson D, Wentzel A, Nieselt K, Ellingsen T, Moore J, Morrissey E, Legaie R,

Wohlleben W, Rodriguez-Garcia A, Wentzel A, Sletta H, Consortium S, Ellingsen T, Bruheim P, Waldvogel E, Herbig A, Battke F, Amin R, Nentwich M, Nieselt K, Ellingsen T, Wentzel A, Hodgson D, Wohlleben W, Mast Y, Claessen D, Rink R, Jong W de, Siebring J, Vreugd P de, Boersma F, Dijkhuizen L, Wosten H, Bystrykh L, Fernandez-Moreno M, Herrema J, Malpartida F, Hopwood D, Dijkhuizen L, Villas-Boas S, Delicado D, Akesson M, Nielsen J, Christensen B, Nielsen J, Strauch E, Takano E, Baylis H, Bibb M, Martin J, Martin J, Demain A, Coisne S, Béchet M, Blondeau R, Gesheva V, Ivanova V, Gesheva R, Nakamura T, Yoshimoto A, Rollins M, Jensen S, Westlake D, Gorst-Allman C, Rudd B, Chang C-J, Floss H, Wasserman H, Shaw C, Sykes R, Cushley R, Bruheim P, Butler M, Ellingsen T, Jonsbu E, Christensen B, Nielsen J, Gunnarsson N, Bruheim P, Nielsen J, Rodriguez-Garcia A, Sola-Landa A, Apel K, Santos-Beneit F, Martin J, Santos-Beneit F, Rodriguez-Garcia A, Sola-Landa A, Martin J, Lambert R, Stratford M, Surowitz K, Pfister R. 2012. Optimized submerged batch fermentation strategy for systems scale studies of metabolic switching in Streptomyces coelicolor A3(2). BMC Systems Biology 6:59.

21. Wentzel A, Sletta H, Consortium S, Ellingsen TE, Bruheim P. 2012. Intracellular Metabolite Pool Changes in Response to Nutrient Depletion Induced Metabolic Switching in Streptomyces coelicolor. Metabolites 2:178–194.

22. Hu H, Zhang Q, Ochi K. 2002. Activation of Antibiotic Biosynthesis by Specified Mutations in the rpoB Gene (Encoding the RNA Polymerase β Subunit) of Streptomyces lividans. Journal of Bacteriology 184:3984–3991.

23. Braesel J, Tran TA, Eustáquio AS. 2019. Heterologous expression of the diazaquinomycin biosynthetic gene cluster. J Ind Microbiol Biotechnol.

24. Kepplinger B, Morton-Laing S, Seistrup KH, Marrs ECL, Hopkins AP, Perry JD, Strahl H, Hall MJ, Errington J, Allenby NEE. 2018. Mode of Action and Heterologous Expression of the Natural Product Antibiotic Vancoresmycin. ACS Chem Biol 13:207–214.

25. Li T, Du Y, Cui Q, Zhang J, Zhu W, Hong K, Li W. 2013. Cloning, Characterization and Heterologous Expression of the Indolocarbazole Biosynthetic Gene Cluster from Marine-Derived Streptomyces sanyensis FMA. Marine Drugs 11:466–488.

26. Battke F, Symons S, Nieselt K. 2010. Mayday--integrative analytics for expression data. BMC Bioinformatics 11:121.

27. Jäger G, Battke F, Nieselt K. 2011. TIALA — Time series alignment analysis, p. 55–61. *In* 2011 IEEE Symposium on Biological Data Visualization (BioVis).

28. Liao Y, Smyth GK, Shi W. 2014. featureCounts: an efficient general purpose program for assigning sequence reads to genomic features. Bioinformatics 30:923–930.

29. Love MI, Huber W, Anders S. 2014. Moderated estimation of fold change and dispersion for RNA-seq data with DESeq2. Genome Biol 15:550.

30. Mi H, Muruganujan A, Ebert D, Huang X, Thomas PD. 2019. PANTHER version 14: more genomes, a new PANTHER GO-slim and improvements in enrichment analysis tools. Nucleic Acids Res 47:D419–D426.

31. Sánchez BJ, Zhang C, Nilsson A, Lahtvee P-J, Kerkhoven EJ, Nielsen J. 2017. Improving the phenotype predictions of a yeast genome-scale metabolic model by incorporating enzymatic constraints. Molecular Systems Biology 13:935.

32. Robinson JL, Nielsen J. 2016. Integrative analysis of human omics data using biomolecular networks. Mol Biosyst 12:2953–2964.

33. Borodina I, Krabben P, Nielsen J. 2005. Genome-scale analysis of Streptomyces coelicolor A3(2) metabolism. Genome research 15:820–9.

34. Alam MT, Merlo ME, (stream) TSC, Hodgson DA, Wellington EM, Takano E, Breitling R. 2010. Metabolic modeling and analysis of the metabolic switch in Streptomyces coelicolor. BMC Genomics 11:202.

35. Amara A, Takano E, Breitling R. 2018. Development and validation of an updated computational model of Streptomyces coelicolor primary and secondary metabolism. BMC Genomics 19:519.

36. Kim MW, Sang Yi J, Kim J-NJJ-NNJ, Kim J-NJJ-NNJ, Kim MW, Kim B-GG. 2014. Reconstruction of a high-quality metabolic model enables the identification of gene overexpression targets for enhanced antibiotic production in streptomyces coelicolor A3(2). Biotechnology Journal 9:1185–1194.

37. Wang H, Marcišauskas S, Sánchez BJ, Domenzain I, Hermansson D, Agren R, Nielsen J, Kerkhoven EJ. 2018. RAVEN 2.0: A versatile toolbox for metabolic network reconstruction and a case study on Streptomyces coelicolor. PLOS Computational Biology 14:e1006541.

38. Mohite OS, Weber T, Kim HU, Lee SY. 2019. Genome-Scale Metabolic Reconstruction of Actinomycetes for Antibiotics Production. Biotechnology Journal 14:1800377.

39. Toro L, Pinilla L, Avignone-Rossa C, Ríos-Estepa R. 2018. An enhanced genome-scale metabolic reconstruction of Streptomyces clavuligerus identifies novel strain improvement strategies. Bioprocess Biosyst Eng 41:657–669.

40. Licona-Cassani C, Marcellin E, Quek L-E, Jacob S, Nielsen LK. 2012. Reconstruction of the Saccharopolyspora erythraea genome-scale model and its use for enhancing erythromycin production. Antonie van Leeuwenhoek 102:493–502.

41. Valverde JR, Gullón S, Mellado RP. 2018. Modelling the metabolism of protein secretion through the Tat route in Streptomyces lividans. BMC Microbiology 18:59.

42. Lieven C, Beber ME, Olivier BG, Bergmann FT, Ataman M, Babaei P, Bartell JA, Blank LM, Chauhan S, Correia K, Diener C, Dräger A, Ebert BE, Edirisinghe JN, Faria JP, Feist A, Fengos G, Fleming RMT, Garcia-Jimenez B, Hatzimanikatis V, Helvoirt W van, Henry C, Hermjakob H, Herrgard MJ, Kim HU, King Z, Koehorst JJ, Klamt S, Klipp E, Lakshmanan M, Novere NL, Lee D-Y, Lee SY, Lee S, Lewis NE, Ma H, Machado D, Mahadevan R, Maia P, Mardinoglu A, Medlock GL, Monk J, Nielsen J, Nielsen LK, Nogales J, Nookaew I, Resendis O, Palsson B, Papin JA, Patil KR, Poolman M, Price ND, Richelle A, Rocha I, Sanchez B, Schaap P, Sheriff RSM, Shoaie S, Sonnenschein N, Teusink B, Vilaca P, Vik JO, Wodke JA, Xavier JC, Yuan Q, Zakhartsev M, Zhang C. 2018. Memote: A community-driven effort towards a standardized genome-scale metabolic model test suite. bioRxiv 350991.

43. Thiele I, Swainston N, Fleming RMT, Hoppe A, Sahoo S, Aurich MK, Haraldsdottir H, Mo ML, Rolfsson O, Stobbe MD, Thorleifsson SG, Agren R, Bölling C, Bordel S, Chavali AK, Dobson P, Dunn WB, Endler L, Hala D, Hucka M, Hull D, Jameson D, Jamshidi N, Jonsson JJ, Juty N, Keating S, Nookaew I, Le Novère N, Malys N, Mazein A, Papin JA, Price ND, Selkov E, Sigurdsson MI, Simeonidis E, Sonnenschein N, Smallbone K, Sorokin A, van Beek JHGM, Weichart D, Goryanin I, Nielsen J, Westerhoff HV, Kell DB, Mendes P, Palsson BØ. 2013. A community-driven global reconstruction of human metabolism. Nat Biotechnol 31.

44. Aung HW, Henry SA, Walker LP. 2013. Revising the Representation of Fatty Acid, Glycerolipid, and Glycerophospholipid Metabolism in the Consensus Model of Yeast Metabolism. Industrial Biotechnology 9:215–228.

45. Dobson PD, Smallbone K, Jameson D, Simeonidis E, Lanthaler K, Pir P, Lu C, Swainston N, Dunn WB, Fisher P, Hull D, Brown M, Oshota O, Stanford NJ, Kell DB, King RD, Oliver SG, Stevens RD, Mendes P. 2010. Further developments towards a genome-scale metabolic model of yeast. BMC Syst Biol 4:145.

46. Heavner BD, Smallbone K, Barker B, Mendes P, Walker LP. 2012. Yeast 5 – an expanded reconstruction of the Saccharomyces cerevisiae metabolic network. BMC Systems Biology 6:55.

47. Heavner BD, Smallbone K, Price ND, Walker LP. 2013. Version 6 of the consensus yeast metabolic network refines biochemical coverage and improves model performance. Database (Oxford) 2013:bat059.

48. Herrgård MJ, Swainston N, Dobson P, Dunn WB, Arga KY, Arvas M, Blüthgen N, Borger S, Costenoble R, Heinemann M, Hucka M, Le Novère N, Li P, Liebermeister W, Mo ML, Oliveira AP, Petranovic D, Pettifer S, Simeonidis E, Smallbone K, Spasić I, Weichart D, Brent R, Broomhead DS, Westerhoff HV, Kırdar B, Penttilä M, Klipp E, Palsson BØ, Sauer U, Oliver SG, Mendes P, Nielsen J, Kell DB. 2008. A consensus yeast metabolic network reconstruction obtained from a community approach to systems biology. Nat Biotechnol 26:1155–1160.

49. Lu H, Li F, Sánchez BJ, Zhu Z, Li G, Domenzain I, Marcišauskas S, Anton PM, Lappa D, Lieven C, Beber ME, Sonnenschein N, Kerkhoven EJ, Nielsen J. 2019. A consensus S. cerevisiae metabolic model Yeast8 and its ecosystem for comprehensively probing cellular metabolism. Nat Commun 10:1–13.

50. Hefzi H, Ang KS, Hanscho M, Bordbar A, Ruckerbauer D, Lakshmanan M, Orellana CA, Baycin-Hizal D, Huang Y, Ley D, Martinez VS, Kyriakopoulos S, Jiménez NE, Zielinski DC, Quek L-E, Wulff T, Arnsdorf J, Li S, Lee JS, Paglia G, Loira N, Spahn PN, Pedersen LE, Gutierrez JM, King ZA, Lund AM, Nagarajan H, Thomas A, Abdel-Haleem AM, Zanghellini J, Kildegaard HF, Voldborg BG, Gerdtzen ZP, Betenbaugh MJ, Palsson BO, Andersen MR, Nielsen LK, Borth N, Lee D-Y, Lewis NE. 2016. A Consensus Genome-scale Reconstruction of Chinese Hamster Ovary Cell Metabolism. Cell Systems 3:434-443.e8.

51. Kanehisa M. 2000. KEGG: Kyoto Encyclopedia of Genes and Genomes. Nucleic Acids Research 28:27–30.

52. Kanehisa M, Sato Y, Furumichi M, Morishima K, Tanabe M. 2019. New approach for understanding genome variations in KEGG. Nucleic Acids Research 47:D590–D595.

53. Karp PD, Billington R, Caspi R, Fulcher CA, Latendresse M, Kothari A, Keseler IM, Krummenacker M, Midford PE, Ong Q, Ong WK, Paley SM, Subhraveti P. 2017. The BioCyc collection of microbial genomes and metabolic pathways. Brief Bioinform.

54. Hastings J, Owen G, Dekker A, Ennis M, Kale N, Muthukrishnan V, Turner S, Swainston N, Mendes P, Steinbeck C. 2016. ChEBI in 2016: Improved services and an expanding collection of metabolites. Nucleic Acids Res 44:D1214–D1219.

55. Moretti S, Martin O, Van Du Tran T, Bridge A, Morgat A, Pagni M. 2016. MetaNetX/MNXref – reconciliation of metabolites and biochemical reactions to bring together genome-scale metabolic networks. Nucleic Acids Res 44:D523–D526.

56. King ZA, Lu J, Dräger A, Miller P, Federowicz S, Lerman JA, Ebrahim A, Palsson BO, Lewis NE, J. H. 2016. BiGG Models: A platform for integrating, standardizing and sharing genome-scale models. Nucleic Acids Research 44:D515–D522.

57. The UniProt Consortium. 2019. UniProt: a worldwide hub of protein knowledge. Nucleic Acids Res 47:D506–D515.

58. Thiele I, Palsson BØ. 2010. A protocol for generating a high-quality genome-scale metabolic reconstruction. Nature protocols 5:93–121.

59. Flamholz A, Noor E, Bar-Even A, Milo R. 2012. eQuilibrator—the biochemical thermodynamics calculator. Nucleic Acids Res 40:D770–D775.

60. Chakrabarty AM. 1998. Nucleoside diphosphate kinase: role in bacterial growth, virulence, cell signalling and polysaccharide synthesis. Molecular Microbiology 28:875–882.

61. Yoshida M, Muneyuki E, Hisabori T. 2001. ATP synthase — a marvellous rotary engine of the cell. Nat Rev Mol Cell Biol 2:669–677.

62. Getsin I, Nalbandian GH, Yee DC, Vastermark A, Paparoditis PC, Reddy VS, Saier MH. 2013. Comparative genomics of transport proteins in developmental bacteria: Myxococcus xanthus and Streptomyces coelicolor. BMC Microbiol 13:279.

63. Smirnov A, Esnault C, Prigent M, Holland IB, Virolle M-J. 2015. Phosphate Homeostasis in Conditions of Phosphate Proficiency and Limitation in the Wild Type and the phoP Mutant of Streptomyces lividans. PLoS One 10.

64. Orth JD, Thiele I, Palsson BØO. 2010. What is flux balance analysis? Nat Biotech 28:245–248.

65. Bordel S, Agren R, Nielsen J. 2010. Sampling the Solution Space in Genome-Scale Metabolic Networks Reveals Transcriptional Regulation in Key Enzymes. PLOS Computational Biology 6:e1000859.

66. Martín JF, Santos-Beneit F, Rodríguez-García A, Sola-Landa A, Smith MCM, Ellingsen TE, Nieselt K, Burroughs NJ, Wellington EMH. 2012. Transcriptomic studies of phosphate control of primary and secondary metabolism in Streptomyces coelicolor. Appl Microbiol Biotechnol 95:61–75.

67. Martín-Martín S, Rodríguez-García A, Santos-Beneit F, Franco-Domínguez E, Sola-Landa A, Martín JF. 2018. Self-control of the PHO regulon: the PhoP-dependent protein PhoU controls negatively expression of genes of PHO regulon in *Streptomyces coelicolor*. The Journal of Antibiotics 71:113–122.

68. Sola-Landa A, Moura RS, Martín JF. 2003. The two-component PhoR-PhoP system controls both primary metabolism and secondary metabolite biosynthesis in Streptomyces lividans. Proc Natl Acad Sci U S A 100:6133–6138.

69. Martín JF, Rodríguez-García A, Liras P. 2017. The master regulator PhoP coordinates phosphate and nitrogen metabolism, respiration, cell differentiation and antibiotic biosynthesis: comparison in *Streptomyces coelicolor* and *Streptomyces avermitilis*. The Journal of Antibiotics 70:534–541.

70. Hojati Z, Milne C, Harvey B, Gordon L, Borg M, Flett F, Wilkinson B, Sidebottom PJ, Rudd BAM, Hayes MA, Smith CP, Micklefield J. 2002. Structure, Biosynthetic Origin, and Engineered Biosynthesis of Calcium-Dependent Antibiotics from Streptomyces coelicolor. Chemistry & Biology 9:1175–1187.

71. Khanin R, Vinciotti V, Mersinias V, Smith CP, Wit E. 2007. Statistical reconstruction of transcription factor activity using Michaelis-Menten kinetics. Biometrics 63:816–823.

72. Santos-Beneit F, Rodríguez-García A, Sola-Landa A, Martín JF. 2009. Cross-talk between two global regulators in Streptomyces: PhoP and AfsR interact in the control of afsS, pstS and phoRP transcription. Molecular Microbiology 72:53–68.

73. Allenby NEE, Laing E, Bucca G, Kierzek AM, Smith CP. 2012. Diverse control of metabolism and other cellular processes in Streptomyces coelicolor by the PhoP transcription factor: genome-wide identification of in vivo targets. Nucleic Acids Res 40:9543–9556.

74. Esnault C, Dulermo T, Smirnov A, Askora A, David M, Deniset-Besseau A, Holland I-B, Virolle M-J. 2017. Strong antibiotic production is correlated with highly active oxidative metabolism in Streptomyces coelicolor M145. Scientific Reports 7:200.

75. Borodina I, Siebring J, Zhang J, Smith CP, Keulen G van, Dijkhuizen L, Nielsen J. 2008. Antibiotic Overproduction in Streptomyces coelicolor A3(2) Mediated by Phosphofructokinase Deletion. J Biol Chem 283:25186–25199.

76. Jonsbu E, Christensen B, Nielsen J. 2001. Changes of in vivo fluxes through central metabolic pathways during the production of nystatin by Streptomyces noursei in batch culture. Appl Microbiol Biotechnol 56:93–100.

77. Stirrett K, Denoya C, Westpheling J. 2009. Branched-chain amino acid catabolism provides precursors for the Type II polyketide antibiotic, actinorhodin, via pathways that are nutrient dependent. J Ind Microbiol Biotechnol 36:129–137.

78. Gallo G, Renzone G, Alduina R, Stegmann E, Weber T, Lantz AE, Thykaer J, Sangiorgi F, Scaloni A, Puglia AM. 2010. Differential proteomic analysis reveals novel links between primary metabolism and antibiotic production in Amycolatopsis balhimycina. PROTEOMICS 10:1336–1358.

79. Coze F, Gilard F, Tcherkez G, Virolle M-J, Guyonvarch A. 2013. Carbon-Flux Distribution within Streptomyces coelicolor Metabolism: A Comparison between the Actinorhodin-Producing Strain M145 and Its Non-Producing Derivative M1146. PLOS ONE 8:e84151.

80. Vinogradov AD, Grivennikova VG. 2016. Oxidation of NADH and ROS production by respiratory complex I. Biochimica et Biophysica Acta (BBA) - Bioenergetics 1857:863–871.

81. Ashburner M, Ball CA, Blake JA, Botstein D, Butler H, Cherry JM, Davis AP, Dolinski K, Dwight SS, Eppig JT, Harris MA, Hill DP, Issel-Tarver L, Kasarskis A, Lewis S, Matese JC, Richardson JE, Ringwald M, Rubin GM, Sherlock G. 2000. Gene ontology: tool for the unification of biology. The Gene Ontology Consortium. Nat Genet 25:25–29.

82. The Gene Ontology Consortium. 2019. The Gene Ontology Resource: 20 years and still GOing strong. Nucleic Acids Res 47:D330–D338.

83. Stahl W, Sies H. 2003. Antioxidant activity of carotenoids. Molecular Aspects of Medicine 24:345–351.

84. Latifi A, Ruiz M, Zhang C-C. 2009. Oxidative stress in cyanobacteria. FEMS Microbiol Rev 33:258–278.

85. Zangar RC, Davydov DR, Verma S. 2004. Mechanisms that regulate production of reactive oxygen species by cytochrome P450. Toxicology and Applied Pharmacology 199:316–331.

86. Lamb DC, Ikeda H, Nelson DR, Ishikawa J, Skaug T, Jackson C, Omura S, Waterman MR, Kelly SL. 2003. Cytochrome P450 complement (CYPome) of the avermectin-producer Streptomyces avermitilis and comparison to that of Streptomyces coelicolor A3(2). Biochemical and Biophysical Research Communications 307:610–619.

87. Bednarz B, Kotowska M, Pawlik KJ. 2019. Multi-level regulation of coelimycin synthesis in Streptomyces coelicolor A3(2). Appl Microbiol Biotechnol 103:6423–6434.

88. Li X, Wang J, Li S, Ji J, Wang W, Yang K. 2015. ScbR- and ScbR2-mediated signal transduction networks coordinate complex physiological responses in *Streptomyces coelicolor*. Scientific Reports 5:14831.

89. Lee P-C, Umeyama T, Horinouchi S. 2002. afsS is a target of AfsR, a transcriptional factor with ATPase activity that globally controls secondary metabolism in Streptomyces coelicolor A3(2). Molecular Microbiology 43:1413–1430.

90. Wolański M, Donczew R, Kois-Ostrowska A, Masiewicz P, Jakimowicz D, Zakrzewska-Czerwińska J. 2011. The Level of AdpA Directly Affects Expression of Developmental Genes in Streptomyces coelicolor ▿. J Bacteriol 193:6358–6365.

91. Naseer N, Shapiro JA, Chander M. 2014. RNA-Seq analysis reveals a six-gene SoxR regulon in Streptomyces coelicolor. PLoS ONE 9:e106181.

92. Dela Cruz R, Gao Y, Penumetcha S, Sheplock R, Weng K, Chander M. 2010. Expression of the Streptomyces coelicolor SoxR regulon is intimately linked with actinorhodin production. J Bacteriol 192:6428–6438.

93. Shin J-H, Singh AK, Cheon D-J, Roe J-H. 2011. Activation of the SoxR regulon in Streptomyces coelicolor by the extracellular form of the pigmented antibiotic actinorhodin. J Bacteriol 193:75–81.

94. Sivapragasam S, Grove A. 2019. The Link between Purine Metabolism and Production of Antibiotics in Streptomyces. Antibiotics (Basel) 8.

95. Hauryliuk V, Atkinson GC, Murakami KS, Tenson T, Gerdes K. 2015. Recent functional insights into the role of (p)ppGpp in bacterial physiology. Nat Rev Microbiol 13:298–309.

96. Hesketh A, Chen WJ, Ryding J, Chang S, Bibb M. 2007. The global role of ppGpp synthesis in morphological differentiation and antibiotic production in Streptomyces coelicolor A3(2). Genome Biol 8:R161.

97. Srivatsan A, Wang JD. 2008. Control of bacterial transcription, translation and replication by (p)ppGpp. Current Opinion in Microbiology 11:100–105.

98. Coze F, Gilard F, Tcherkez G, Virolle M-J, Guyonvarch A. 2013. Carbon-Flux Distribution within Streptomyces coelicolor Metabolism: A Comparison between the Actinorhodin-Producing Strain M145 and Its Non-Producing Derivative M1146. PLoS ONE 8:e84151.

99. Chemler JA, Buchholz TJ, Geders TW, Akey DL, Rath CM, Chlipala GE, Smith JL, Sherman DH. 2012. Biochemical and Structural Characterization of Germicidin Synthase: Analysis of a Type III Polyketide Synthase that Employs Acyl-ACP as a Starter Unit Donor. J Am Chem Soc 134:7359–7366.

100. Lopatniuk M, Ostash B, Luzhetskyy A, Walker S, Fedorenko V. 2014. Generation and study of the strains of streptomycetes – heterologous hosts for production of moenomycin. Russ J Genet 50:360–365.

101. Craney A, Ozimok C, Pimentel-Elardo SM, Capretta A, Nodwell JR. 2012. Chemical Perturbation of Secondary Metabolism Demonstrates Important Links to Primary Metabolism. Chemistry & Biology 19:1020–1027.

102. Xu J, Tozawa Y, Lai C, Hayashi H, Ochi K. 2002. A rifampicin resistance mutation in the rpoB gene confers ppGpp-independent antibiotic production in Streptomyces coelicolor A3(2). Mol Gen Genomics 268:179–189.

103. Jones G, Sol RD, Dudley E, Dyson P. 2011. Forkhead-associated proteins genetically linked to the serine/threonine kinase PknB regulate carbon flux towards antibiotic biosynthesis in Streptomyces coelicolor. Microbial Biotechnology 4:263–274.

104. Kim D-J, Huh J-H, Yang Y-Y, Kang C-M, Lee I-H, Hyun C-G, Hong S-K, Suh J-W. 2003. Accumulation of S-Adenosyl-l-Methionine Enhances Production of Actinorhodin but Inhibits Sporulation in Streptomyces lividans TK23. Journal of Bacteriology 185:592–600.

105. Okamoto S, Lezhava A, Hosaka T, Okamoto-Hosoya Y, Ochi K. 2003. Enhanced Expression of S-Adenosylmethionine Synthetase Causes Overproduction of Actinorhodin in Streptomyces coelicolor A3(2). Journal of Bacteriology 185:601–609.

106. Rodriguez E, Navone L, Casati P, Gramajo H. 2012. Impact of Malic Enzymes on Antibiotic and Triacylglycerol Production in Streptomyces coelicolor. Appl Environ Microbiol 78:4571–4579.

107. Liu G, Chater KF, Chandra G, Niu G, Tan H. 2013. Molecular Regulation of Antibiotic Biosynthesis in Streptomyces. Microbiol Mol Biol Rev 77:112–143.

108. van den Berg MA, Albang R, Albermann K, Badger JH, Daran J-M, Driessen AJM, Garcia-Estrada C, Fedorova ND, Harris DM, Heijne WHM, Joardar V, Kiel JAKW, Kovalchuk A, Martín JF, Nierman WC, Nijland JG, Pronk JT, Roubos JA, van der Klei IJ, van Peij NNME, Veenhuis M, von Döhren H, Wagner C, Wortman J, Bovenberg RAL. 2008. Genome sequencing and analysis of the filamentous fungus *Penicillium chrysogenum*. Nature Biotechnology 26:1161–1168.

109. Crook N, Alper H. 2012. Classical strain improvement. Engineering complex phenotypes in industrial strains. John Wiley & Sons, Inc) http://dx doi org/101002/9781118433034 ch1 Daniell, J, Nagaraju, S, Burton, F, Köpke, M, and Simpson, SD (2016) Low-Carbon Fuel and Chemical Production by Anaerobic Gas Fermentation Adv Biochem Eng Biotechnol 156:293–321.

110. Takano E, Chakraburtty R, Nihira T, Yamada Y, Bibb MJ. 2001. A complex role for the γ-butyrolactone SCB1 in regulating antibiotic production in Streptomyces coelicolor A3(2). Molecular Microbiology 41:1015–1028.

111. van Dissel D, Claessen D, Roth M, van Wezel GP. 2015. A novel locus for mycelial aggregation forms a gateway to improved Streptomyces cell factories. Microbial Cell Factories 14:44.

112. Courtot M, Juty N, Knüpfer C, Waltemath D, Zhukova A, Dräger A, Dumontier M, Finney A, Golebiewski M, Hastings J, Hoops S, Keating S, Kell DB, Kerrien S, Lawson J, Lister A, Lu J, Machne R, Mendes P, Pocock M, Rodriguez N, Villeger A, Wilkinson DJ, Wimalaratne S, Laibe C, Hucka M, Le Novère N. 2011. Controlled vocabularies and semantics in systems biology. Mol Syst Biol 7:543.

113. Noor E, Haraldsdóttir HS, Milo R, Fleming RMT. 2013. Consistent Estimation of Gibbs Energy Using Component Contributions. PLOS Computational Biology 9:e1003098.

114. Bar-Even A, Flamholz A, Noor E, Milo R. 2012. Thermodynamic constraints shape the structure of carbon fixation pathways. Biochimica et Biophysica Acta (BBA) - Bioenergetics 1817:1646–1659.

115. Feist AM, Henry CS, Reed JL, Krummenacker M, Joyce AR, Karp PD, Broadbelt LJ, Hatzimanikatis V, Palsson BØ. 2007. A genome-scale metabolic reconstruction for Escherichia coli K-12 MG1655 that accounts for 1260 ORFs and thermodynamic information. Molecular Systems Biology 3:121.

116. Elbourne LDH, Tetu SG, Hassan KA, Paulsen IT. 2017. TransportDB 2.0: a database for exploring membrane transporters in sequenced genomes from all domains of life. Nucleic Acids Research 45:D320–D324.

117. Saier MH, Reddy VS, Tsu BV, Ahmed MS, Li C, Moreno-Hagelsieb G. 2016. The Transporter Classification Database (TCDB): recent advances. Nucleic Acids Res 44:D372–D379.

118. NCBI Resource Coordinators. 2017. Database Resources of the National Center for Biotechnology Information. Nucleic Acids Research 45:D12–D17.

119. Jeske L, Placzek S, Schomburg I, Chang A, Schomburg D. 2019. BRENDA in 2019: a European ELIXIR core data resource. Nucleic Acids Res 47:D542–D549.

120. Fritzemeier CJ, Hartleb D, Szappanos B, Papp B, Lercher MJ. 2017. Erroneous energy-generating cycles in published genome scale metabolic networks: Identification and removal. PLOS Computational Biology 13:e1005494.

121. Noor E. 2018. Removing both Internal and Unrealistic Energy-Generating Cycles in Flux Balance Analysis. arXiv:180304999 [q-bio].

122. Haraldsdóttir HS, Cousins B, Thiele I, Fleming RMT, Vempala S. 2017. CHRR: coordinate hit-and-run with rounding for uniform sampling of constraint-based models. Bioinformatics 33:1741–1743.

123. Kaufman DE, Smith RL. 1998. Direction Choice for Accelerated Convergence in Hit-and-Run Sampling. Operations Research 46:84–95.

124. Megchelenbrink W, Huynen M, Marchiori E. 2014. optGpSampler: An Improved Tool for Uniformly Sampling the Solution-Space of Genome-Scale Metabolic Networks. PLOS ONE 9:e86587.

125. Kieser T, Bibb MJ, Buttner M, Chater K, Hopwood DA. 2000. Practical Streptomyces Genetics. John Innes Foundation, Norwich, UK.

126. Claessen D, Rink R, Jong W de, Siebring J, Vreugd P de, Boersma FGH, Dijkhuizen L, Wösten HAB. 2003. A novel class of secreted hydrophobic proteins is involved in aerial hyphae formation in Streptomyces coelicolor by forming amyloid-like fibrils. Genes Dev 17:1714–1726.

127. Bystrykh LV, Fernández-Moreno MA, Herrema JK, Malpartida F, Hopwood DA, Dijkhuizen L. 1996. Production of actinorhodin-related “blue pigments” by Streptomyces coelicolor A3(2). J Bacteriol 178:2238–2244.

128. Wessel D, Flügge UI. 1984. A method for the quantitative recovery of protein in dilute solution in the presence of detergents and lipids. Anal Biochem 138:141–143.

129. Rappsilber J, Mann M, Ishihama Y. 2007. Protocol for micro-purification, enrichment, pre-fractionation and storage of peptides for proteomics using StageTips. Nat Protoc 2:1896–1906.

130. Distler U, Kuharev J, Navarro P, Levin Y, Schild H, Tenzer S. 2014. Drift time-specific collision energies enable deep-coverage data-independent acquisition proteomics. Nat Methods 11:167–170.

131. Andrews S. 2016. FastQC: a quality control tool for high throughput sequence data.

132. Kim D, Langmead B, Salzberg SL. 2015. HISAT: a fast spliced aligner with low memory requirements. Nat Methods 12:357–360.

133. Li H, Handsaker B, Wysoker A, Fennell T, Ruan J, Homer N, Marth G, Abecasis G, Durbin R, 1000 Genome Project Data Processing Subgroup. 2009. The Sequence Alignment/Map format and SAMtools. Bioinformatics 25:2078–2079.

134. Okonechnikov K, Conesa A, García-Alcalde F. 2016. Qualimap 2: advanced multi-sample quality control for high-throughput sequencing data. Bioinformatics 32:292–294.

135. Battke F, Nieselt K. 2011. Mayday SeaSight: combined analysis of deep sequencing and microarray data. PLoS ONE 6:e16345.

136. Huang DW, Sherman BT, Lempicki RA. 2009. Bioinformatics enrichment tools: paths toward the comprehensive functional analysis of large gene lists. Nucleic Acids Res 37:1–13.

137. Huang DW, Sherman BT, Lempicki RA. 2009. Systematic and integrative analysis of large gene lists using DAVID bioinformatics resources. Nat Protoc 4:44–57.

138. Szklarczyk D, Gable AL, Lyon D, Junge A, Wyder S, Huerta-Cepas J, Simonovic M, Doncheva NT, Morris JH, Bork P, Jensen LJ, Mering C von. 2019. STRING v11: protein-protein association networks with increased coverage, supporting functional discovery in genome-wide experimental datasets. Nucleic Acids Res 47:D607–D613.

139. Perez-Riverol Y, Csordas A, Bai J, Bernal-Llinares M, Hewapathirana S, Kundu DJ, Inuganti A, Griss J, Mayer G, Eisenacher M, Pérez E, Uszkoreit J, Pfeuffer J, Sachsenberg T, Yilmaz S, Tiwary S, Cox J, Audain E, Walzer M, Jarnuczak AF, Ternent T, Brazma A, Vizcaíno JA. 2019. The PRIDE database and related tools and resources in 2019: improving support for quantification data. Nucleic Acids Res 47:D442–D450.